New Jersey Institute of Technology
Digital Commons @ NJIT

Theses | Theses and Dissertations

Fall 2016

Real time, integrated, paper based temperature sensor for lab on a chip device

Vignesh Shekhar
New Jersey Institute of Technology

Follow this and additional works at: https://digitalcommons.njit.edu/theses

 Part of the Chemical Engineering Commons

Recommended Citation
Shekhar, Vignesh, "Real time, integrated, paper based temperature sensor for lab on a chip device" (2016). *Theses*. 10.
https://digitalcommons.njit.edu/theses/10

This Thesis is brought to you for free and open access by the Theses and Dissertations at Digital Commons @ NJIT. It has been accepted for inclusion in Theses by an authorized administrator of Digital Commons @ NJIT. For more information, please contact digitalcommons@njit.edu.

Copyright Warning & Restrictions

The copyright law of the United States (Title 17, United States Code) governs the making of photocopies or other reproductions of copyrighted material.

Under certain conditions specified in the law, libraries and archives are authorized to furnish a photocopy or other reproduction. One of these specified conditions is that the photocopy or reproduction is not to be "used for any purpose other than private study, scholarship, or research." If a, user makes a request for, or later uses, a photocopy or reproduction for purposes in excess of "fair use" that user may be liable for copyright infringement,

This institution reserves the right to refuse to accept a copying order if, in its judgment, fulfillment of the order would involve violation of copyright law.

Please Note: The author retains the copyright while the New Jersey Institute of Technology reserves the right to distribute this thesis or dissertation

Printing note: If you do not wish to print this page, then select "Pages from: first page # to: last page #" on the print dialog screen

NJIT New Jersey's Science & Technology University

The Van Houten library has removed some of the personal information and all signatures from the approval page and biographical sketches of theses and dissertations in order to protect the identity of NJIT graduates and faculty.

ABSTRACT

REAL TIME, INTEGRATED, PAPER BASED TEMPERATURE SENSOR FOR LAB ON A CHIP DEVICE

by
Vignesh Shekhar

Temperature measurement and manipulation is a critical factor in a wide range of applications like Point Of Care Diagnostics (POC's), Polymerase Chain Reaction (PCR), Temperature Gradient Focusing (TGF) to cite few prominent examples. In the past decade, researchers have used various techniques to sense and control the temperature in microfluidic systems. The primary challenge has been the twin problem of integration and accuracy using minimal equipment while keeping it simple. In this study, an equipment free fabrication of the temperature sensor using filter paper impregnated with p-type colloidal PbS quantum dots is demonstrated. This sensor is later integrated into line a PDMS microfluidic device with two parallel microfluidic channels. The integrated device is chiefly to sense the difference in temperature of fluids inside the two channels. COMSOL Multiphysics 5.1 is used to simulate the single-phase laminar fluid flow and heat transfer in the microchannel of the device. The design of the microfluidic channel is optimized to decrease heat sensing times of the sensor using the simulation results.

REAL TIME, INTEGRATED, PAPER BASED TEMPERATURE SENSOR FOR LAB ON A CHIP DEVICE

by
Vignesh Shekhar

A Thesis
Submitted to the Faculty of
New Jersey Institute of Technology
in Partial Fulfillment of the Requirements for the Degree of
Master of Science in Chemical Engineering

Otto H. York Department of
Chemical, Biological and Pharmaceutical Engineering

January 2017

APPROVAL PAGE

REAL TIME, INTEGRATED, PAPER BASED TEMPERATURE SENSOR FOR LAB ON A CHIP DEVICE

Vignesh Shekhar

Dr. Sagnik Basuray, Thesis Advisor — Date
Assistant Professor of Chemical Engineering, NJIT

Dr. Robert B. Barat, Committee Member — Date
Professor of Chemical Engineering, NJIT

Dr. Laurent Simon, Committee Member — Date
Associate Professor of Chemical Engineering, NJIT

Dr. Dong Kyun Ko, Committee Member — Date
Assistant Professor of Electrical and Computer Engineering, NJIT

BIOGRAPHICAL SKETCH

Author: Vignesh Shekhar

Degree: Master of Science

Date: January 2017

Undergraduate and Graduate Education:

- Master of Science in Chemical Engineering,
  New Jersey Institute of Technology, Newark, NJ, 2017

- Bachelor of Technology in Chemical Engineering,
  Anna University, Chennai, India, 2015

Major: Chemical Engineering

I dedicate this thesis to all my loved ones;
Family, friends and my cute little niece, Vibha.

ACKNOWLEDGMENT

First of all, I offer my heartfelt gratefulness to my thesis advisor, Dr. Sagnik Basuray, who has backed me from start to finish of my thesis with his composure and proficiency at the same time allowing me to perform in my own way. I associate the level of my Master's degree to his optimism and effort and without him my thesis too, would not have been brought about or written.

I wish to thank my committee members: Dr. Robert B. Barat, Dr. Laurent Simon, and Dr. Dong Kyun Ko, for freely offering their time, support, guidance and good will throughout the preparation and review of this thesis. Thank you for investing time and giving helpful feedback. I feel glad and honored that you have accepted to be on my committee.

On another note, I am very grateful to Dr. Dong Kyun Ko again and Dr. Chengjun Sun for providing me with the materials I needed for my project on time. Your impressive work has been the basis of my project.

Also, I like to acknowledge Hathija Noor, who taught me from scratch and backed me at every step of my work. I am very grateful for the help and guidance of my fellow lab mates, Dr. Bhuvana Mohanlal, Nida Riaz, Mehnaz Mursalat, Andrew House, and Victoria Harbour, through my research.

Finally, this would not have been possible without the support of my beloved parents, sister and friends.

TABLE OF CONTENTS

TABLE OF CONTENTS
(Continued)

LIST OF TABLES

LIST OF FIGURES

LIST OF FIGURES
(Continued)

Figure **Page**

LIST OF FIGURES
(Continued)

Figure **Page**

CHAPTER 1

INTRODUCTION

1.1 Microfluidics

Microfluidics is primarily the handling of fluids at the micron level which requires both a deep knowledge of physics of fluids at the microscale and fabrication of the devices with microchannels (Whitesides, 2006). The general aim behind microfluidics is to integrate multiple unit operations that are undertaken in an analytical lab in a single chip.

The advantages of microfluidics are: Reduction in size, high surface to volume ratio, handling less amounts of fluids, reduced consumption of chemical reagents, low power consumption, safety, portability, ability to work with small quantities, increase in speed of reaction, integration with other devices – lab on a chip, ease of disposing devices and fluids (Nge, Rogers, & Woolley, 2013). Hence, microfluidics has been chiefly used to develop technologies that improve capabilities of researchers in medical research and biology such as Point of care diagnostics (POC's)(Jung, Han, Choi, & Ahn, 2015), cell analysis(Yeo et al., 2016), biosensing, and drug development(Kang, Chung, Langer, & Khademhosseini, 2008). Also, in many studies, methods are described to replace macro scale assays wherein 'proof of concept' experiments are conducted on microfluidic systems to find out the efficiency of a new approach (Sackmann, Fulton, & Beebe, 2014).

Integration is one of the main benefits of miniaturization and paves the way for assays for point of care (POC) usage(Nge et al., 2013). Lab-on-a-chip systems integrate multiple lab processes into a single device like biochemical reactions(Lee, Lee Cs Fau - Kim, Kim Bg Fau - Kim, & Kim), separation and detection(Baek, Kim, Na, & Min, 2015),

polymerase chain reaction(Oblath, Henley, Alarie, & Ramsey, 2013). Researchers have made significant progress toward this objective over the last decade. Integration on the chip reduces sample loss and analysis time. Further, integration can be anywhere from a disposable chip in an external equipment to full integration of all lab processes.

The present study deals with integrating real-time temperature sensing element in a microfluidic device for various applications like on-chip polymerase chain reaction (PCR).

1.2 Sensor and Diagnostics

In the recent past, paper as a substrate has attracted much attention as the main material for sensors in clinical diagnosis, quality monitoring, and environmental supervision because of its low cost, adaptability and ample supply(Nery & Kubota, 2013). These sensors can be integrated into ways that are adjustable, movable, dispensable and easy to use. With soaring costs in health care, there is an increasing need for a point of care (POC) device for rapid diagnostics. Paper-based sensors have shown great potential in meeting this critical need (Liana, Raguse, Gooding, & Chow, 2012). The current study, introduces a paper based temperature sensor for lab on a chip device. Paper sensors for temperature control and sensing in microfluidic systems offer several advantages over current methods, which will be discussed in detail next.

A wide range of techniques(Miralles, Huerre, Malloggi, & Jullien, 2013) have been developed and used for temperature regulation within microfluidic systems. For example, external heating or cooling methods like Peltier elements have been developed (Chon & Li, 2008). Others include preheated liquids(Houssin et al., 2016), integration of

temperature regulating elements using microwaves(Morgan et al., 2013), lasers (liquid directly heated in bulk material)(Hung, Ho, & Chen, 2016), Joule heating(Erickson, Sinton D Fau - Li, & Li), chemical reactions(Singleton et al., 2013) and integrated wires(Bertrand Selva, Mary, & Jullien, 2010). The external and bulk temperature control methods have proven to be advantageous for specific applications like, rapid PCR analysis, providing on chip temperature gradients and micro-valve functioning. Though these elements have shown impressive accuracy, these methods are not considered as an integrated microfluidic system. Further, these elements have a large size (range of mm). However, many applications need accurate temperature measurements and precise control. Hence, the present study's focus is on the integration of temperature sensing elements into a microfluidic device.

Guijt, Dodge, van Dedem, de Rooij, and Verpoorte (2003), used exothermic and endothermic reactions to control the temperature in microchannel. This is fully integrated and cost effective too. For cooling, the latent heat during the evaporation of acetone is used and for heating 97 wt% Sulphuric Acid (H_2SO_4) is used. A fluorescent dye is used to measure and monitor the temperature. The authors tuned flow rate ratios of the chemical reactants to regulate the temperature by adjusting the intensity of the reaction.

Xue and Qiu (2005), have introduced a method to integrate micromachined temperature sensor array in a glass microchannel. They use a modified anodic bonding technique to bond two different glass materials. They also performed channel etching and fabricated silicon temperature detectors. These methods make it possible for them to fabricate a glass microchannel with integrated temperature detector array.

Vigolo, Rusconi, Stone, and Piazza (2010), reported a technique based on Joule heating which depends on the conductivity of metals or liquids. Heating resistors are embedded in the microfluidic systems, and a direct relationship can be achieved between the used power and the heat flux.

Pitchaimani et al. , tapped PDMS's ability to deform with temperature changes. He developed a PDMS based chip which would act as a thermally actuated plastic microfluidic valve. The fluid flow was kept under control using a temperature sensitive fluid in the plastic valve which would deflect a thin elastomeric film. They made the heaters by depositing 100 nm gold film by sputtering on the plastic film, and by applying power to it they controlled flow rates.

De Mello, Habgood, Lancaster, Welton, and Wootton (2004), used joule heated ionic fluids flowing through serpentine-like geometry microchannels providing direct control of internal temperature easily. This geometry was studied by Lao, Lee, Hsing, and Ip (2000), with integrated platinum heaters and sensors digitally feedback controlled, allowing precise temperature control and providing quick response times.

In 2009 a microheater was designed by Wu, Cao, Wen, Chang, and Sheng (2009), along with a thermal sensor directly by injecting silver paste into a PDMS microchannels and integrating metal wires. They developed multiple serpentine geometry and heated the silver paste in three steps: 60, 100, 150 ℃ and sensed the temperature by measuring the resistance in the integrated wire.

Darhuber, Davis, Troian, and Reisner (2003), developed a device with micro heaters made of Ti metal which is coupled to the glass substrate. This is done using chemical patterning and is actuated electronically. Due to thermocapillary actuation; they

control the formation, displacement, bonding, and breaking of droplets on demand with excellent accuracy.

B. Selva, Jullien, Miralles, and Cantat (2010), worked in creating thermo-mechanical effects due to PDMS dilation and thermal capillarity. An increase in temperature brought out competing phenomena in microfluidics for the first time. They reported a bubble/drop displacement, trapping and switching based on thermo-mechanical effect using long PDMS capillaries and resistive heaters.

Vigolo et al. (2010), reported a method to drive particles toward a hot or cold side by the addition of special electrolytes to the initial solution. They fabricated a device where temperature gradients were imposed by the combination of epoxy resistors and preheated liquid on both sides of channels. They implement the use of polystyrene beads to see the collection of particles in cold side by fluorescence.

The thermal gradient was used for alternative heating of two heaters in a study conducted by Kim, Wang, Burns, and Kurabayashi (2009). Further this enables micro-mixing without a pump. They made heaters from Pt/Ti alloy and used fluorescent beads as tracers to find out the steady state flow speed.

Table 1.1 gives a summary of techniques adopted in integrated temperature regulation for lab on chip systems in the last 16 years.

Table 1.1 Summary of Integrated Temperature Sensing and Control Methods Applied in the Last 16 Years

AUTHOR	METHOD	ELEMENTS	SPECIFICATIONS
Guijt et al. (2003)	Chemical Reaction	Two reagents for heating and cooling	Temp range: -3 to 76°C, 1°C/s ramp
Bertrand Selva et al. (2010)	Joule heating (homogeneous temperature)	Resistor, fluorescent dye	25 - 96°C, 0.6°C , 20°C/s ramp, 300 mW power
Vigolo et al. (2010)	Joule heating (temperature gradient)	Silver filled epoxy	25-75°C, 20°C/s ramp, 1000 mW, 2°C accuracy
Pitchaimani et al.	Thermal actuation of plastic valves	Temperature sensing fluid, PCB controller	Heater power: 36 mW – 80 mW
De Mello et al. (2004)	Joule heating (homogeneous temperature)	Thermocouples, ionic liquids	20--130°C, 0.1°C/s ramp, 0.2°C accuracy, 1000 mW
Lao et al. (2000)	Joule heating (homogeneous temperature)	Platinum heaters and sensors, control algorithm and feedback PI scheme	50-100°C, +20 -10°C/s ramp, 1°C accuracy, 2200 mW
Wu et al. (2009)	Joule heating (homogeneous temperature)	Micro-heaters, Feedback system	PCR carried out in 25 cycles at 1min/cycle
Darhuber et al. (2003)	Thermocapillary effect	Microheater arrays, chemical surface patterning	Breakup of droplet on demand, single micro heater applied power 5-200 W
B. Selva et al. (2010)	Thermo-mechanical effect	Optimized resistor patterning	<0.4 W, first-time observance of competing phenomena in microfluidics
Vigolo et al. (2010)	Thermophoresis (temperature gradient)	Electrolytes, liquid/epoxy resistors	Selective driving of particles by addition of electrolytes
Kim et al. (2009)	Micromixing (temperature gradient)	Microfabricated heating instrument	Pump-less micro-mixing by alternative heating cycles

1.3 Current Disadvantages in Temperature Sensing

A wide variety of technologies has been implemented in the past decade to obtain integrated temperature control. These techniques pose different advantages or drawbacks on the degree of integration, cost, space utilized, and accuracy. The drawbacks of current temperature sensing involve complex fabrication, bigger elements, usage of reagents/dyes to control and sense temperature, costly methods, lower integration/accuracy.

Given the current disadvantages in temperature sensing, the present study deals with a cheap, hassle-free fabrication of an on chip paper based temperature sensor. This paper-based device can be used for heating by applying a potential difference. As both the microfluidic device and the sensor/heater is made of PDMS and paper respectively, the overall integrated microfluidic device is cost-effective. The heat transfer coupled with laminar flow in the microchannel is simulated using COMSOL Multiphysics 5.1 to optimize the micro channel's design to decrease the sensing times based on flow rates, corresponding residence times and various depths of the cavity in the microchannel.

1.4 PDMS – The Material of Choice

Materials such as glass, silicon, and polymers like Polydimethylsiloxane (PDMS), Polystyrene (PS), Polymethylmethacrylate (PMMA) and Polycarbonate (PC) have been used over the years to fabricate microfluidic devices (Nge et al., 2013). Clearly, there is no 'perfect' material as each one of them has some benefits and drawbacks when used in microfluidics. Finally, it is the application which helps the researcher to decide which material to use in the construction of the device.

In this study, Polydimethylsiloxane (PDMS) is used to fabricate the microfluidic device due to the following benefits (McDonald et al., 2000):

- Micron-scale structures can be fabricated with a large constancy in PDMS by Soft lithography.
- PDMS is visually transparent and can be used for various detection techniques.
- Low-temperature curing is possible with PDMS, and it is not toxic.
- It can seal to itself and other materials reversibly by Van der Waals bonding.
- It seals irreversibly after plasma-air exposure through covalent bonding.
- PDMS is elastomeric and forms smooth, nonplanar surfaces.
- It detaches itself from fine features of a mold without any damage.
- It is cheaper than other materials used in manufacturing microfluidic devices.
- PDMS has very low thermal conductivity (~0.2 W/mK) (McDonald et al., 2000) which is beneficial to the study here.

These advantages that PDMS provides, paves the way to build a microfluidic device with ease, without any equipment and to efficiently integrate a paper sensor into it.

1.5 Motivation and Thesis Outline

The disadvantages in the temperature sensing/heating in the lab-on-a-chip systems is the motivation behind the current study. The present study overcomes these disadvantages and brings out a cheap, efficient, and optimized lab-on-a -chip paper based thermal sensor using a simple fabrication technique. The optimization of the microchannel to improve the sensitivity of the sensor is carried out by simulating the fluid flow and heat transfer inside the microchannel using COMSOL Multiphysics 5.1.

Here we detail the fabrication protocol, simulation, optimization and experimental verification of the integrated temperature sensor. In Chapter 1, an introduction to microfluidics coupled with the importance of integrating processes onto a chip is touched upon. A review of methods developed in the past 16 years in the field of temperature sensing and control in microfluidics is also presented. The disadvantages of these methods are revealed and how the current study nullifies these disadvantages is pointed out. At the end of this chapter, the materials used to fabricate microfluidic systems is identified, and PDMS is selected due to its various advantages.

In Chapter 2, the protocol to fabricate the paper based temperature sensor along with the integration of this sensor in a microfluidic device by soft lithography is demonstrated. The problem statement – the optimization of the microchannel design is discussed at the end of this chapter.

In Chapter 3, various geometries that are considered in this study along with the assumptions, boundary conditions, initial conditions and material properties are detailed. Further, these are used in a model to solve the Navier-Stokes, continuity and heat equations. The assumptions and boundary conditions are also supported with relevant literature. This chapter also discusses the solution methodology followed in COMSOL Multiphysics 5.1 which involves meshing and solving by the finite element method. Results from the simulation are presented and a simple calibration model is discussed at the end of Chapter 3. Lastly, Chapter 4 includes a summary and conclusions derived from the simulation results and suggestions for future work in developing an explosive sensor on a chip are discussed.

CHAPTER 2

DEVICE

This chapter details the simple protocol to fabricate a cost-effective, flexible temperature sensor based on cellulose papers and colloidal semiconductor quantum dots. Further, the particulars in the fabrication of the microfluidic device that integrates the paper sensor with a PDMS device is shown.

2.1 Temperature Sensor Fabrication

The work of Sun, Goharpey, Rai, Zhang, and Ko (2016) was followed in the preparation of paper strips impregnated in colloidal PbS quantum dots for temperature sensing which involves the following steps: Standard air-free Schlenk line technique is used to synthesize 8.1 nm PbS quantum dots. A 50 mL three neck flask is used to combine 0.446 g of PbO (99.999%) and 20 mL of oleic acid (tech grade, 90%). This mixture is stirred, dried at 110 °C in vacuum for 2-3 hours to obtain a clear solution. Nitrogen is filled in the flask and solution temperature is increased to 150 °C and then 0.2 mL of hexamethyldisilazane (synthesis grade) in 10 mL of 1-octadecene (90%) is promptly infused. The temperature of the mixture quickly drops to 120 °C. For 16 minutes the reaction temperature is controlled at 120 ± 6 °C and is stopped using a water bath. The dispersion of the quantum dots is done in hexane, acetone is used in the precipitation, and Nitrogen filled glove box is used for centrifugation. After doing the purification step twice, the quantum dots are re-distributed and stored in hexane. A 50 mg/mL PbS quantum dots solution is used to dip a filter paper (Whatman 40, 2.5 X 1.0 cm). The filter paper is then

dipped into 0.1 M KOH in methanol solution for a minute, and the ligand exchange procedure is brought about. Later, this filter paper strip is flushed with ample amount of methanol to remove free residual ligands. A layer by layer method is used for the ligand exchange process and is repeated 15 times. Finally, the temperature sensing paper strip is obtained which is later integrated into the microfluidic device described in the next section.

2.2 PDMS Device Fabrication

This section explains the process of making the PDMS microfluidic device with the paper-based temperature sensor by soft lithography. The Fabrication process of the microfluidic chip is also shown in Figure 2.1 and 2.2. The device fabrication consists of the following steps: 45 grams of PDMS (Sylgard 184) and 4.5 grams of curing agent (Sylgard 184 silicone elastomer kit) (10:1 ratio of PDMS and curing agent) is obtained in a dish and mixed well for five minutes thoroughly. The mixture is placed in a dessicator to remove air bubbles, which approximately takes twenty minutes.

In the meantime, there are three parts to this device which are to be made separately and combined as one final device. Part 1: Glass top – A glass slide is obtained, and four holes are drilled in line with the two ends of the parallel channels in a cricut tape (ARcare-90445 clear polyester double-sided acrylic adhesive (Adhesives Research, Inc.). Using superglue or epoxy, two inlet, and two outlet fluid ports are fixed in their respective holes in the glass slide. Part 2: Microchannels (middle portion) – consists of a cricut tape on which two parallel microchannels are cut using a Cricut Explore One machine. The diameter of the two channels is 500 micrometers and 30 mm in length. Part 3: PDMS

substrate (base) – A paper electrode is obtained, and two pieces of copper wire are cut (~2 inches in length). Electrically conductive silver paint is applied to the two ends of the paper sensor on one side. Two copper wires are pasted to the silver padded ends with conductive

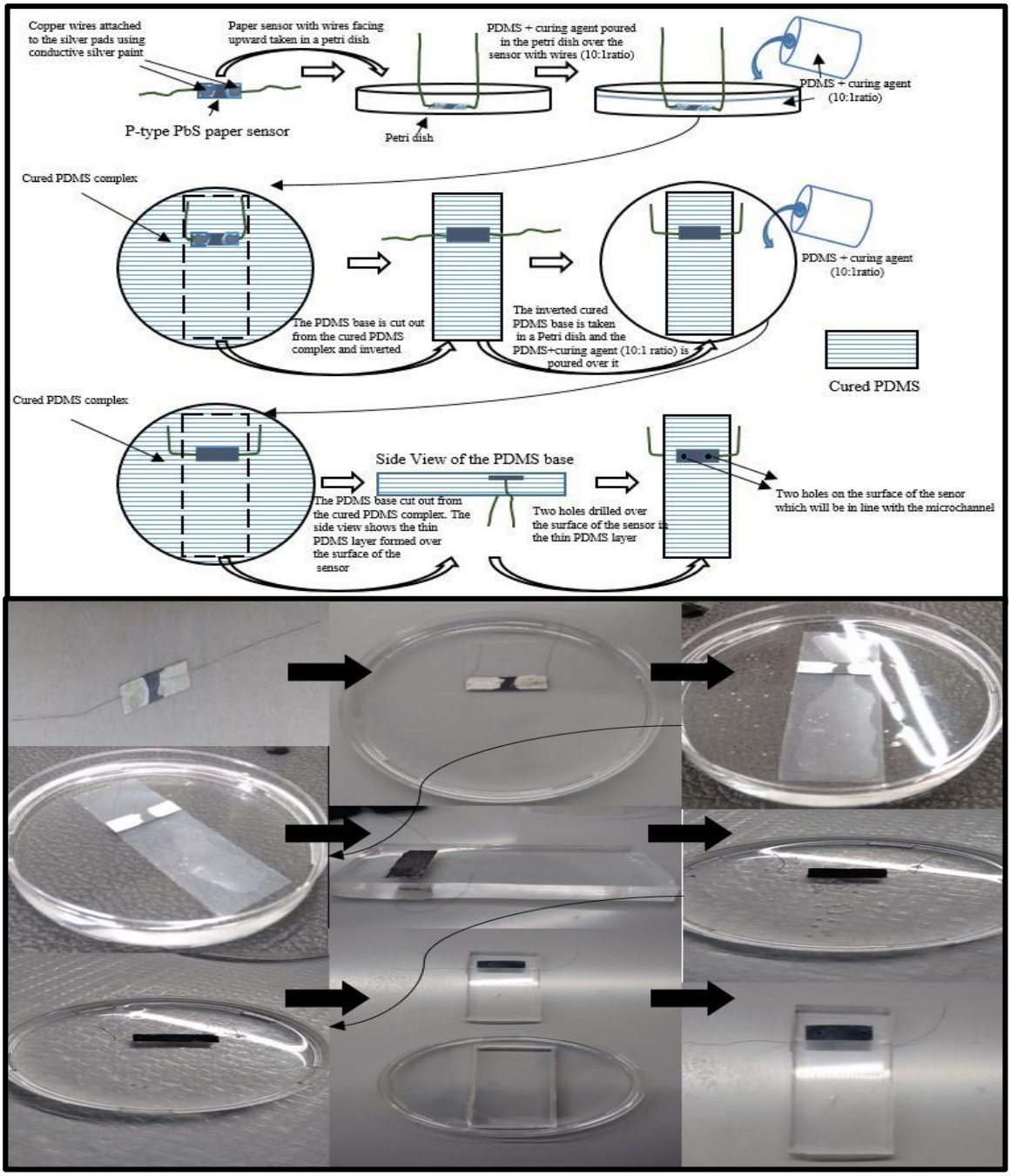

Figure 2.1 The steps in the fabrication process of the PDMS microfluidic device. The paper sensor is prepped with the copper wires first and is immersed in PDMS+curing agent complex. It goes through the curing process twice and finally the PDMS base with the sensor is obtained which is then passed on to the device assembly stage.

silver paint again. The wired paper sensor is taken in a petri dish with the wire side facing upward. The degassed mixture of PDMS is then poured onto the wire portion of the sensor in the petri dish and placed in the degasser again to remove air bubbles.

After degassing, the petri dish contents are cured in a preheated oven for three hours at 70 °C. After curing, the PDMS base is cut out to the shape of the glass slide. This PDMS base is inverted (wire side facing down) and the base is again placed in a petri dish. Now, 45 grams of PDMS and 4.5 grams of the curing agent is obtained and mixed thoroughly for five minutes and degassed in a desiccator to remove air bubbles. The degassed mixture is then poured over the PDMS base in the petri dish. The petri dish contents are then cured at 70 °C for three hours.

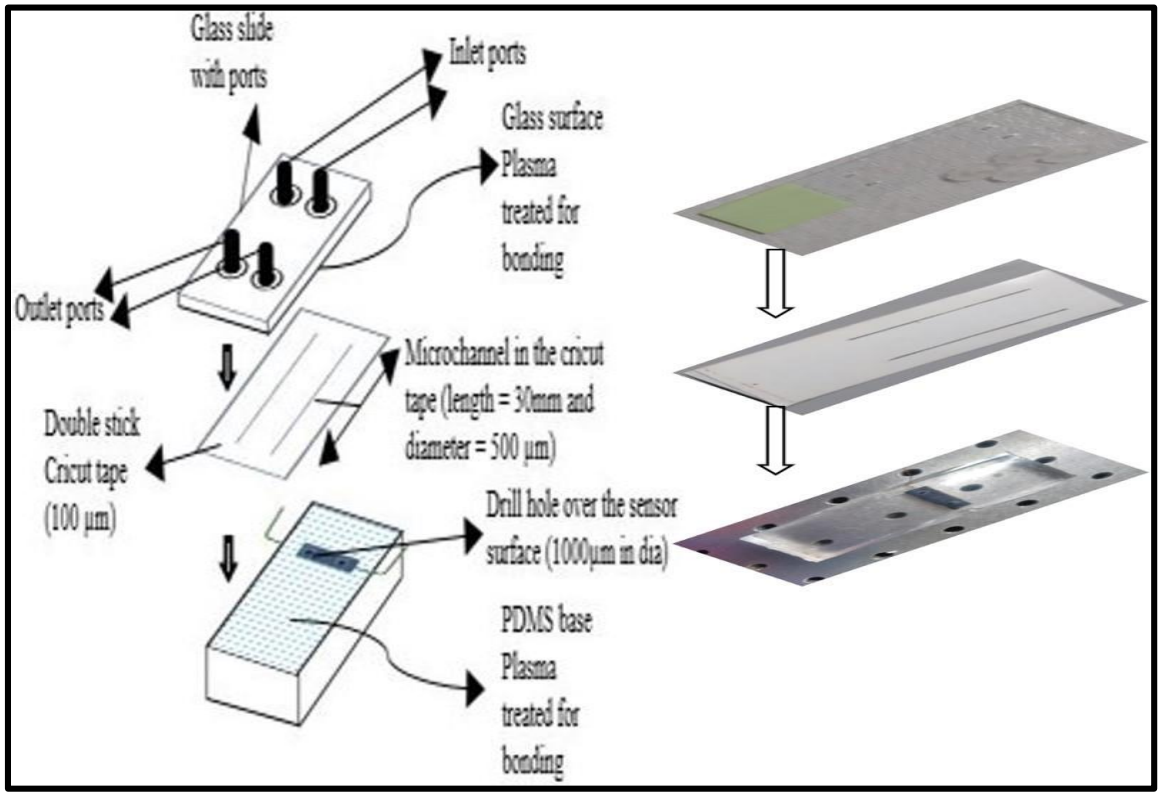

Figure 2.2 Final Assembly of the microfluidic device after preparation of the PDMS base. The PDMS base integrated with the sensor from the soft lithography process is obtained along with the prepared glass slide with ports and the cricut tape. The PDMS base and the glass slide undergo Plasma treatment before assembling the device.

After the curing process, the PDMS is cut out to the shape of the glass slide top. Two holes are made over the surface of the sensor at its two ends in the PDMS layer over which the two microchannels will be placed. Part 4: Final assembly of thermal sensor – The PDMS base, glass top are air-plasma treated before assembling them. The cricut tape containing the channels is stuck on the surface of the PDMS base and is made sure that the channels go over the two holes made on the surface of the paper sensor in the PDMS layer. On top of the cricut tape the glass top with the ports is stuck (the ports need to be in line with the channel). After assembly, this device is flow tested for any leakage before carrying out experimental runs.

2.3 Experimental Setup

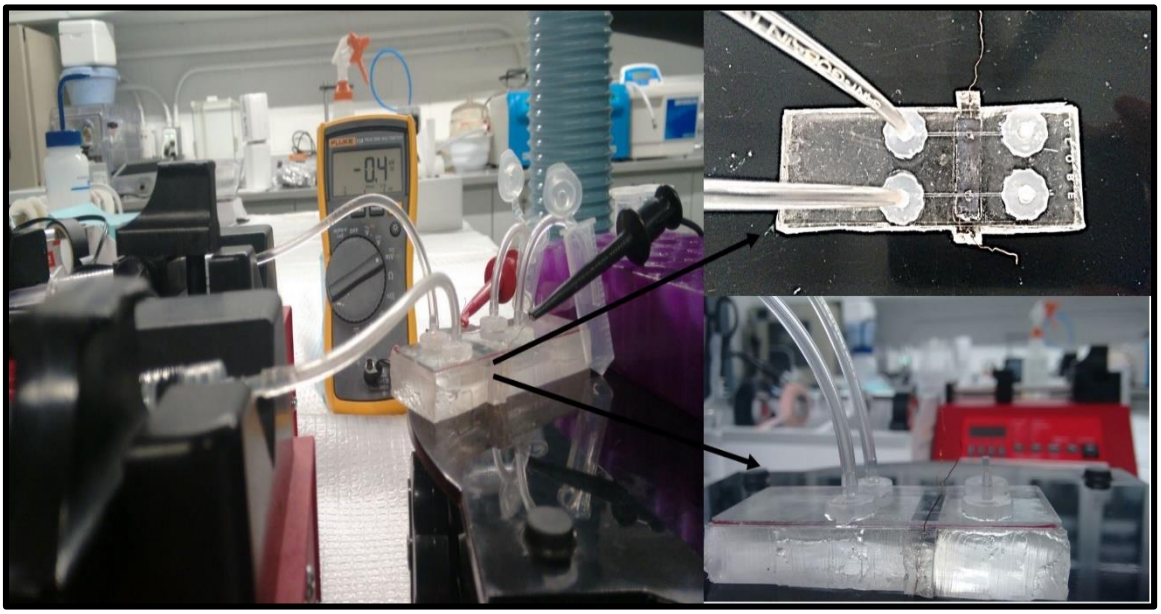

Figure 2.3 Experimental setup of the device. The two inlets of the device are connected to two syringe pumps and the two outlets go into two microcentrifuge tubes. The wires from the paper sensor are attached to a digital multimeter.

Figure 2.3 shows the experimental setup of the microfluidic device. The two inlets of the device are connected to two NE-1000 programmable single syringe pumps through the tubing. The tubing from the outlet goes into two microcentrifuge tubes. The wires of the sensor are attached to an FLUKE-115 Compact digital multimeter.

Deionized water is taken in two 25mL beakers. The beakers are heated or cooled to a required temperature and are maintained at that required temperature. 1mL samples of it are taken in two plastic syringes, and it's placed on the single syringe pumps. Tubing is used to connect with the inlet ports of each channel. The copper wires extending from the device is attached to the digital multimeter. A flow rate is set in the syringe pump and is initiated (preferably 1mL/hr). The initiated run is continued until steady voltage readings are obtained. Before doing another experimental run the flow is stopped, and the sensor is allowed to equilibrate to a voltage reading of zero.

2.4 Optimization

Figure 2.4 shows a simple reproduction of the design of the microfluidic channel inside the PDMS device. Consider a heated fluid at some temperature entering the inlet at some flow rate and flowing through the outlet. To allow the sensor to sense the actual temperature, first of all, the fluid must reach the surface of the sensor inside the cavity along the length of the channel. Second of all, after liquid's contact with the sensor the temperature which the sensor senses is not going to be the same as at the inlet. It is going to take some time for temperature homogeneity to develop all over the channel after heated fluid injection (demonstrated in COMSOL Multiphysics 5.1). The aim here is to optimize the design of

the channel such that the heated fluid makes contact with the sensor easily and also sense the actual temperature quickly (fast sensing times) after injection.

COMSOL Multiphysics 5.1 is employed for the optimization of the channel design by coupling heat transfer and laminar fluid flow phenomena and computing it. The channel dimensions are varied, and the simulation is run to bring about the best design for the channel in which the sensing time of the sensor is the least. In obtaining an optimized design the sensing times, residence times are plotted against various depths of the reservoir above the sensor surface for different flow rates in which a sensing time less than the residence time is sought after. Thereby, a range of the various depths of the reservoir along the channel can be found which have sensing times lesser than the residence times. The COMSOL simulation setup and methodology used will be discussed in the next section.

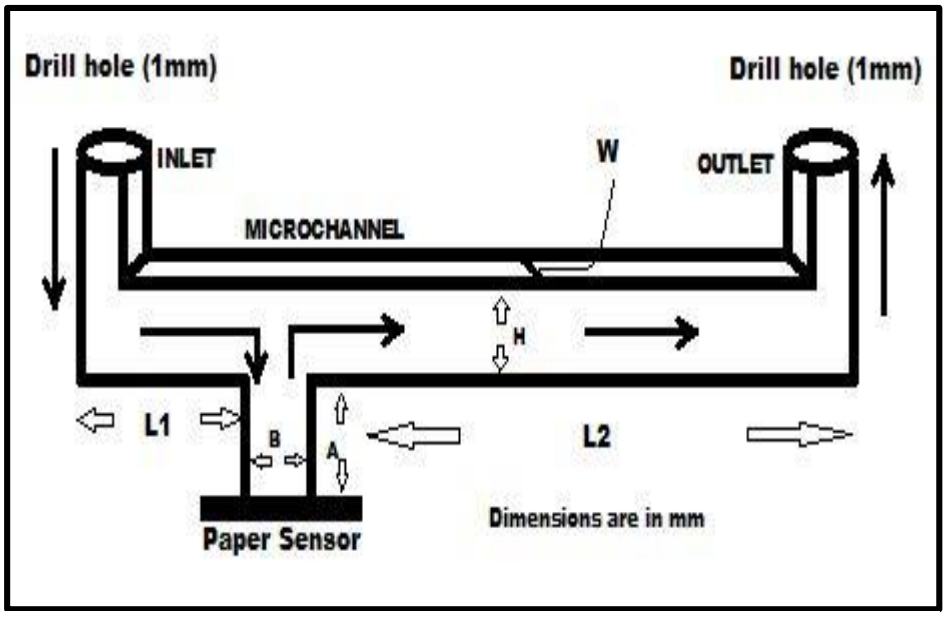

Figure 2.4 Schematic representation of the microfluidic channel in the PDMS device. The arrows represent fluid motion from the inlet to the outlet. L1, L2, a, A, H, W are the length, width and height dimensions of the channel. The objective is to study the heat sensing times of the sensor on changes in dimensions of ‘A,' ‘L1’ and ‘L2’.

CHAPTER 3

COMSOL

The Navier-Stokes, continuity and heat equations need to be solved with the appropriate initial conditions, assumptions and boundary conditions. This section deals with the solution of the governing coupled Navier-Stokes equation with the heat equation. Further, we describe in details the algorithm that is followed in simulating the heat transfer and laminar flow in the microchannel in COMSOL Multiphysics 5.1.

3.1 Mathematical Modeling

In this study, the case considered is single-phase laminar forced convective flow of water in a microchannel with a cavity along its length. Heat transfer by convection is the thermal energy transfer in the presence of a temperature difference as a combination of advection (fluid motion in bulk) and diffusion (random molecular motion). As liquid water is transported through the channels with the help of an external pump, the mechanism of liquid and heat transport is called as forced convection. The velocity components pop up in the convective terms of the energy equation, so the energy equation's solution depends on the converged solution of the flow field.

Liquid water's density does not change appreciably with temperature rise, and thus, mixed convection (forced and free) effects are not considered. The objective of this study is to obtain an optimized design for the microchannel which has lesser sensing times than the residence times. The subsequent sections will focus on the assumptions, initial conditions, boundary conditions, governing equations and steps in COMSOL for setting

up the model and for simulating the laminar flow coupled with heat transfer in the microchannel.

3.1.1 Assumptions and Initial Conditions

Water is considered to be the fluid in the model which undergoes steady, laminar flow in the microchannel. The density of the fluid is taken to be constant, thereby making the incompressible fluid approximation valid. This assumption was also taken in the works of (Khan & Yovanovich, 2008), (Negi, 2013), and (Liu & Garimella, 2005).

Table 3.1 Values for the Material Properties of Water

Property	**Name**	**Value**	**Unit**
Dynamic viscosity	mu	0.0008509	Pa*s
Ratio of specific heats	gamma	1.0	1
Heat capacity at constant pressure	C_p	0.00418	J/(kg*K)
Density	rho	996.59	Kg/m^3
Thermal conductivity	k	0.6	W/(m*K)

Gravitational forces are neglected since the system is horizontal and also that the static pressure under gravity is very low ($P = \rho gh$; $1000kg/m^3*9.81m/s^2*100\mu m = 0.9$ Pa). Tretheway and Meinhart (2002), have shown using particle image velocimetry that the no-slip condition is valid for water flowing through hydrophilic channels. The PDMS microchannel in this study, is hydrophilic due to plasma treatment, thereby making the no-slip assumption valid for the model here. The no-slip assumption was also taken in the works of (Wadgaonkar & Arikapudi), (Patsis, Petropoulos, & Kaltsas, 2012), and (Negi, 2013).

Radiation heat transfer is neglected when compared to convection-diffusion heat transfer (Liu & Garimella, 2005) and insulated boundaries are assumed everywhere except the inlet and outlet boundary (Erickson et al.), (Patsis et al., 2012), (Negi, 2013).

The following are the initial conditions and material properties given for the model: T=300 K, p = 0 Pa, u = 0 m/s similar to the initial conditions taken in (Liu & Garimella, 2005)'s work.

3.1.2 Boundary Conditions

The boundary conditions applied in this model are similar to the boundary conditions adapted in the works of (Wadgaonkar & Arikapudi), (Patsis et al., 2012), (Erickson, Sinton, & Li, 2003), (Negi, 2013). For incompressible flows, velocity inlets and outlets are set. Velocity inlet is used to fix incoming velocities for incompressible flows. The pressure is calculated at the inlet. The velocities: 10^-3, 5*10^-4, 10^-4 and 5*10^-5 m/s are used at the inlet boundary in this model. For heat transfer, an inlet temperature of 323.15K is specified in the model.

To define the outflow a pressure boundary condition is given based on the flow pressure, p_0 (static or gauge pressure) at the outlet of the model. The pressure outlet boundary condition fixes the static pressure at the outlet. In trying to simulate the incompressible fluid flow, there is no way to determine the absolute pressure at any point. Therefore, we start with a guess pressure at the outlet. This is interpreted as the static pressure of the environment into which the flow exhausts. In this model, the static/gauge pressure 'p_0' is set to 0 Pa and the operating pressure 'p_{ref}' is set to 1 atm.

For heat transfer, the outflow boundary condition is selected at the outlet boundary in the model. Outflow conditions are configured to model flow exits where details of flow

velocity and pressure are not known before the solution to flow problem. The outflow fixes the exit at an outflow boundary and intends to represent a smooth continuation of flow through the boundary. The velocity and pressure are calculated. This condition is appropriate where the exit flow is close to a fully developed condition because the outflow condition assumes zero normal gradients for all flow variables except pressure. The solver extrapolates from within the domain and updates the outflow velocity and pressure in a way which is consistent with a fully developed flow. Moreover, an overall mass balance correction is applied.

All walls of the microchannel except the inlet and outlet boundaries in this model have the thermal insulation boundary condition (-n*[k∇T] = 0). Also, the walls are given the no-slip condition which means that the velocity 'u' at the walls of the microchannel is zero.

3.1.3 Governing Equations

The Navier-Stokes equation governs the motion of fluids. For the case of a compressible Newtonian fluid, it gives Equation 3.1 where p is fluid pressure, u is the velocity of the fluid, ρ the fluid density and μ the fluid dynamic viscosity. The term on the left-hand side of Equation 3.1 is the inertial force, the first term on the right is pressure force, and the second term on the right is a viscous force, and the last term on the right is the external forces applied to the fluid. Moreover, Equation 3.2 represents conservation of mass. The first term $\frac{\partial \rho}{\partial t}$ in Equation 3.2 is the change of density with time. This term is cancelled as constant density is assumed in this model. Thus, Equation 3.2 leads to Equation 3.3 which is true for incompressible fluids.

$$\rho \left(\frac{\partial \boldsymbol{u}}{\partial t} + \mathbf{u}.\nabla \boldsymbol{u} \right) = -\nabla p + \nabla . \left(\mu(\nabla \boldsymbol{u} + (\nabla \boldsymbol{u})^{T}) - \frac{2}{3}\mu(\nabla . \boldsymbol{u})\mathbf{I} \right) + \mathbf{F} \quad (3.1)$$

The Navier-Stokes equation is always solved along with the continuity equation:

$$\frac{\partial \rho}{\partial t} + \nabla.(\rho u) = 0 \quad (3.2)$$

The conservation of momentum is represented by Navier-Stokes equation whereas the conservation of mass is represented by the continuity Equation 3.2.

Based on flow regime, it is possible to simplify these equations. In fluid dynamics, different flow regimes are classified using a non-dimensional number, like Reynolds number/ Mach number. The Reynolds number, $Re = \rho UL/\mu$ is the ratio of inertial forces to viscous forces. In this study, the flow is laminar and incompressible. Therefore the continuity Equation 3.2 reduces to Equation 3.3.

$$\nabla . \boldsymbol{u} = 0 \quad (3.3)$$

Also, because of the divergence of the velocity being equal to zero the term, $-\frac{2}{3}\mu(\nabla \boldsymbol{u})\mathbf{I}$ can be removed from the viscous force term in the Navier Stokes equation. Since gravity forces are neglected the external forces term 'F' is also removed from the Navier Stokes equation. Finally, the Navier Stokes equation reduces to Equation 3.4.

$$0 = -\nabla p + \nabla . \left(\mu(\nabla \boldsymbol{u} + (\nabla \boldsymbol{u})^{T}) \right) \quad (3.4)$$

$$\rho C_p \frac{\partial T}{\partial t} + \rho C_p \mathbf{u}.\nabla T + \nabla \mathbf{q} = Q + Q_p + Q_{vd} \; ; \; \mathbf{q} = -k\nabla T \quad (3.5)$$

The heat equation is given by equation 3.5, where C_p is heat capacity of the fluid, Q is the source term, and ρ is fluid density. The first term on the left-hand side represents the heat accumulation term, the second term on the left-hand side represents heat transfer due to bulk fluid motion, q represents Fourier's law for heat conduction and Q_p, Q_{vd} is the work due to pressure changes and viscous dissipation respectively.

In this study, the model is a multiphysics model as it involves more than one kind of physics. The Navier-Stokes equations from fluid dynamics work together with the heat transfer equation. There are four unknowns (dependent variables): the velocity field components, u and v, the pressure, p, and the temperature, T.

The equations are related through bidirectional multiphysics couplings. It involves fluid dynamics coupled with heat transfer. The pressure *p,* and the velocity fields *u* and *v,* are solutions of the Navier-Stokes equations whereas the temperature *T,* is solved using the heat equation. The bidirectional multiphysics couplings relate all these variables.

The above equations are the heart of fluid flow and heat transfer modeling. COMSOL Multiphysics solves those using time-dependent solvers for a particular set of boundary conditions and predicts the above unknown variables for a given geometry. The next section deals with setting up of the model in COMSOL Multiphysics 5.1.

3.2 Method of Solution

When computational fluid dynamics are performed, a good geometric model is the first step to achieve a successful simulation. To do so, first, the relevant physics is chosen in COMSOL Multiphysics 5.1. The single-phase laminar flow and heat transfer in fluids physics are selected along with a time-dependent study. The next thing to do, is to build the geometry. The geometry was manually built in COMSOL. Two global parameters are created which is the depth of the cavity in the microchannel and its position along the length of the microchannel. This makes parametric sweeps possible and provides results using which an optimized design of the microchannel is brought about.

The next step after creating geometry is to add material. Water is added to all the domains of the geometry. The Laminar flow physics node is then selected, and the appropriate boundary conditions are given. The inlet velocity is mentioned after selecting the respective boundary in the geometry. Likewise, the outlet pressure condition (p = 0Pa) is given to the outlet boundary. No slip wall boundary conditions are given everywhere else, and initial conditions are set to zero.

For the Heat transfer in fluids physics node, the same previous process is followed. An inlet temperature is given at the inlet boundary by selecting it, and the temperature outflow (-n.q = 0) is given at the outlet boundary. The zero flux condition is applied at the outlet boundary in fully developed flows and means that the conditions of the outflow plane will be extrapolated from within the domain and have no impact on the upstream flow. The rest of the boundaries are taken to be thermally insulated with initial conditions set to zero.

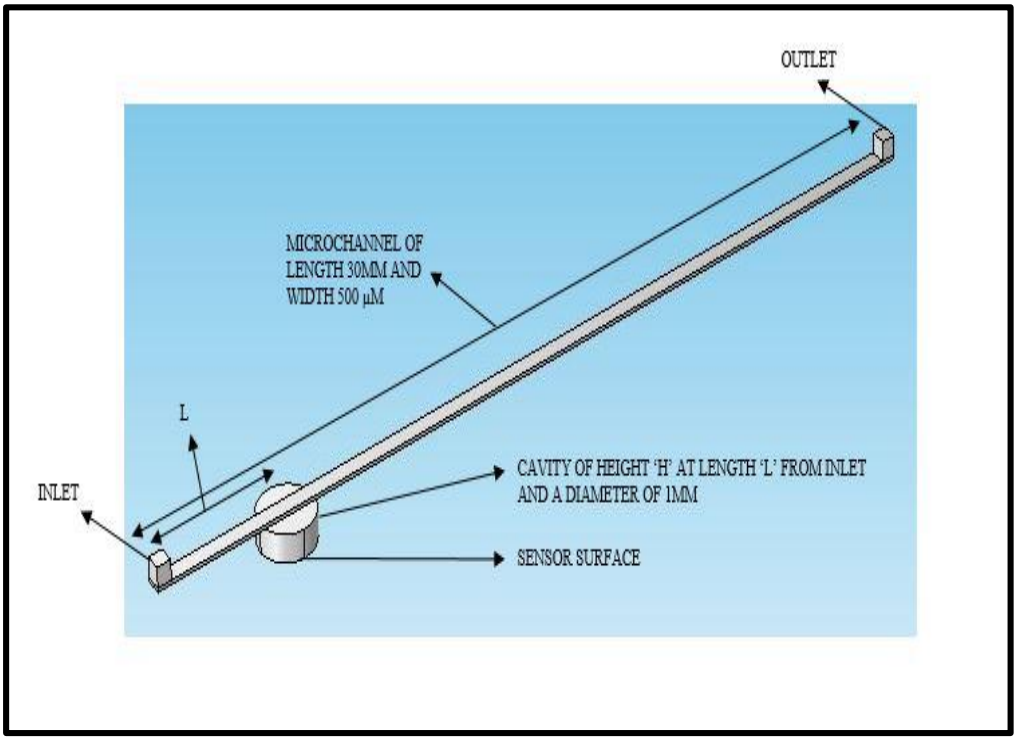

Figure 3.1 Geometry built in COMSOL. The actual representation of the layout of the microchannel in the microfluidic device. The figure shows the dimensions of the channel and the cavity along the length of the channel.

Before making the assumption of having the rest of the boundaries insulated, two types of boundary conditions were tested. First, a constant convective heat flux boundary condition was given to the sensor surface area (at the base of the cavity) alone, based on the resistance in series concept. The heat transfer coefficient of the PbS quantum dot impregnated paper sensor and PDMS was calculated using the ratio of thermal conductivity (k) to its characteristic length (L). The thermal conductivity and characteristic length of the paper sensor were taken as 0.23 W/mK (Sun et al., 2016) and 210 µm (thickness of paper sensor) respectively. For PDMS, values of 0.15 W/mK(McDonald et al., 2000) and 0.01m(thickness of PDMS base) were taken for the thermal conductivity and the characteristic length respectively. The heat transfer coefficient of the paper sensor was found to be 1095.23 W/m^{2}K and that of PDMS was found to be 15 W/m^{2}K.

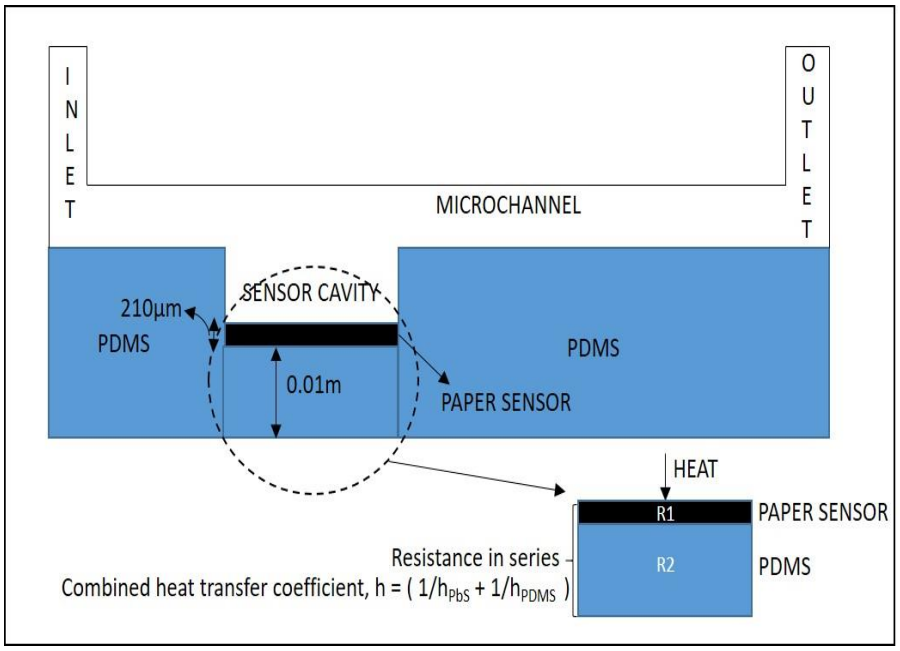

Figure 3.2 The resistance in series concept applied at the sensor boundary. The combined heat transfer coefficient is calculated and applied to the base of the sensor cavity in COMSOL. The combined heat transfer coefficient being 14.79 W/m^{2}K.

Based on the resistance network concept, the combined heat transfer coefficient 'h' is calculated by the formula, $h = (1/h_{PbS} + 1/h_{PDMS})$. The combined heat transfer coefficient was found out to be 14.79 W/m^2K which was entered in the convective heat flux boundary condition in COMSOL.

In the second type of boundary condition, a constant heat flux is applied on all boundaries assuming the whole channel being surrounded by PDMS material. A constant convective heat flux h_{PDMS} = 15 W/m^2K is given to the heat flux boundary condition in COMSOL.

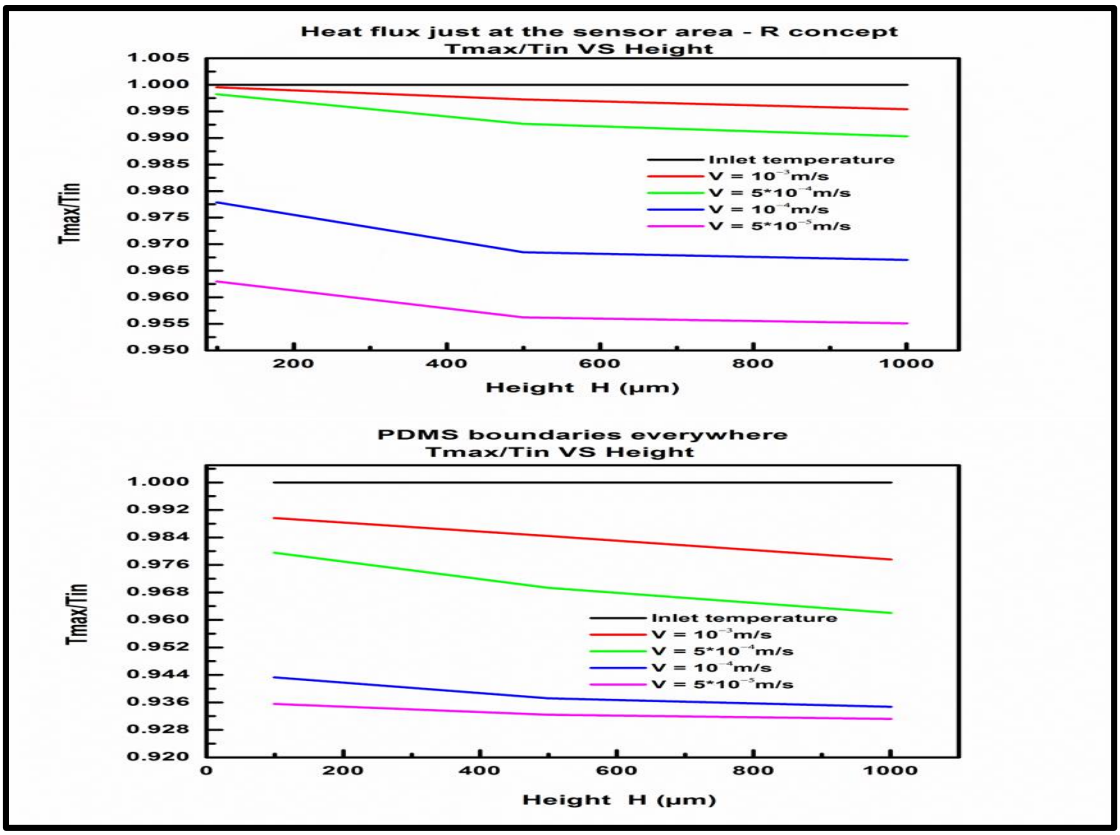

Figure 3.3 T_{max}/T_{in} vs. height plots for the boundary conditions: heat flux just at the sensor boundary (top), heat flux at the sensor and also the walls considering the channel covered with PDMS. The plots show that the inlet temperature does not reach the sensor's surface for both the boundary conditions. The plots were generated with the cavity positioned at L=5000μm, various heights and various velocities. The inlet temperature was set at 323.15K

The simulation is run using these two boundary conditions instead of the insulating boundary condition. Surprisingly, the inlet temperature does not reach the sensor, as seen in Figure 3.3 Therefore, an insulating boundary condition is used at the sensor boundary and also the walls of the microchannel.

The heat transfer in fluids and laminar flow physics are coupled by selecting the Multiphysics coupling node. COMSOL is based on the finite element method approach, which is why meshing is needed to be done after the geometry and physics nodes are prepped. Although there are other methods like finite difference and finite volume to discretize differential equations, a common method for solving the fluidics problems is the finite element method (Shilling, 2001). For any linear or nonlinear system of ordinary differential equations, the finite element method can be outlined as follows. First, the solution domain is discretized by the construction of series of interlocking elements and nodes, which results in a finite number of elements that approximates the spatial geometry. These elements can have different shapes like triangular, tetrahedral, and linear. Then the process involves variational calculus, matrix multiplication, minimization of error functions. This results in a solution for the computational domain at the nodes. In the case of linear elements, linear interpolation between nodes.

In this study, a user defined mesh/selective mesh is selected for the geometry. A finer mesh is given to the base of the cavity in the channel where the paper sensor is present, and an extremely course mesh is given to the rest of the geometry. This selective mesh reduces computational load compared to a geometry which is fully finer meshed. It also provides accurate results with the finer mesh at the sensor area which is the focus of the study here.

Figure 3.5, shows the plot comparison of the maximum temperature at the sensor's surface for a finer mesh versus an extremely coarse mesh. The objective is to find the time at which the sensor's surface reaches the maximum temperature (inlet temperature = 323.15 K). In the case of the physics controlled mesh-extremely coarse mesh everywhere (plot – B in the figure) at the surface of the sensor, the maximum temperature is

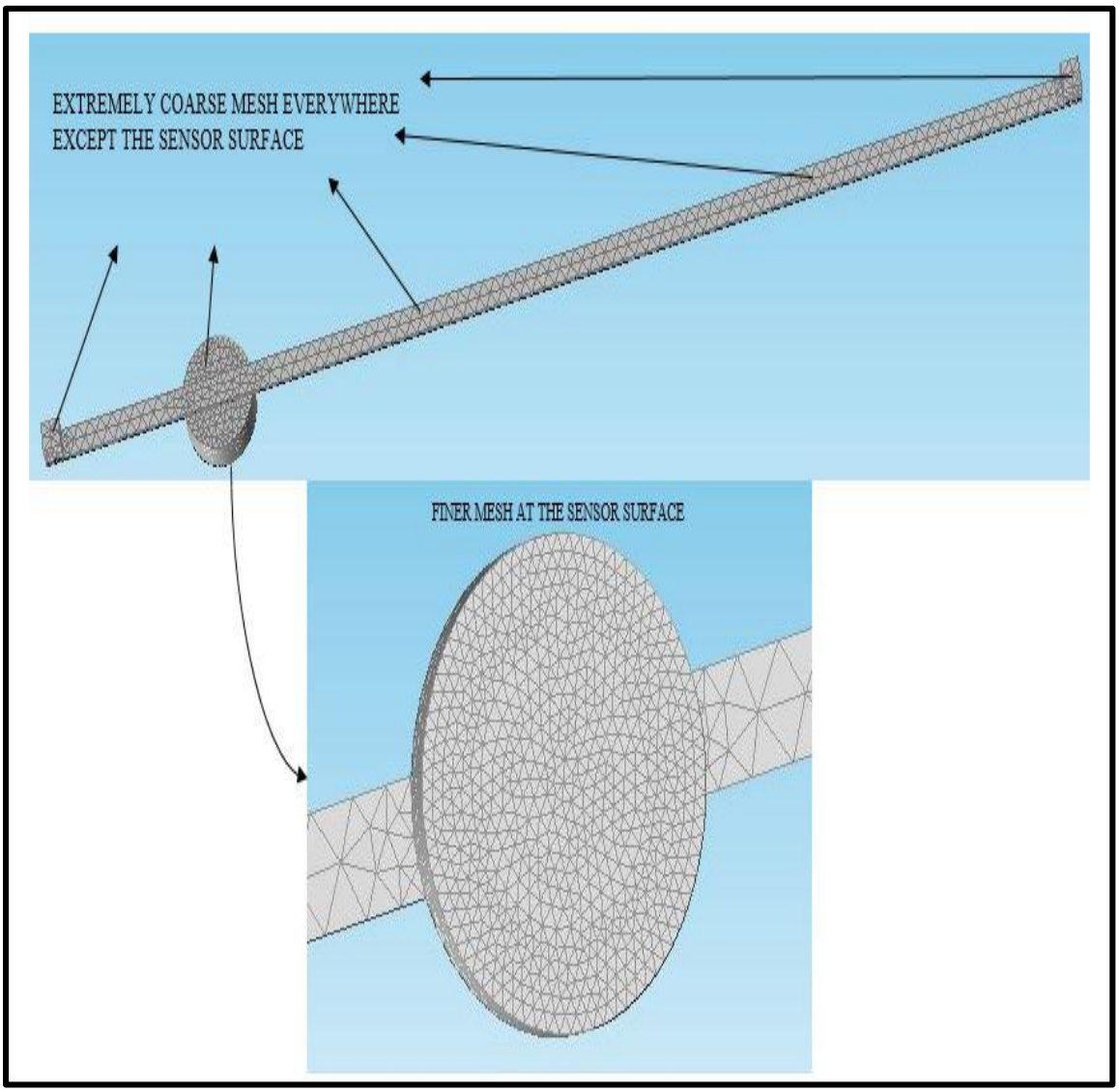

Figure 3.4 Selective user defined meshing of the geometry. The figure shows the comparison of the mesh at the sensor surface (fine) vs. that elsewhere (extremely coarse). The number of nodes are very high on the sensor surface which would produce more accurate results compared to a highly coarse mesh at the sensor surface.

inconclusive due to irregularity, oscillations in the data. Having faced this issue, a user controlled mesh – Finer mesh at the sensor surface, and extremely coarse everywhere was used. Along with this, the time step in the time-dependent study node was changed to 0.1s (previously, 1s), and the solver was made strict (previously, free). These changes gave a plot shown in the figure below (plot – A). The maximum temperature can be recorded easily now as it is steady at 323.15K (inlet temperature) without oscillations, unlike the extremely coarse mesh.

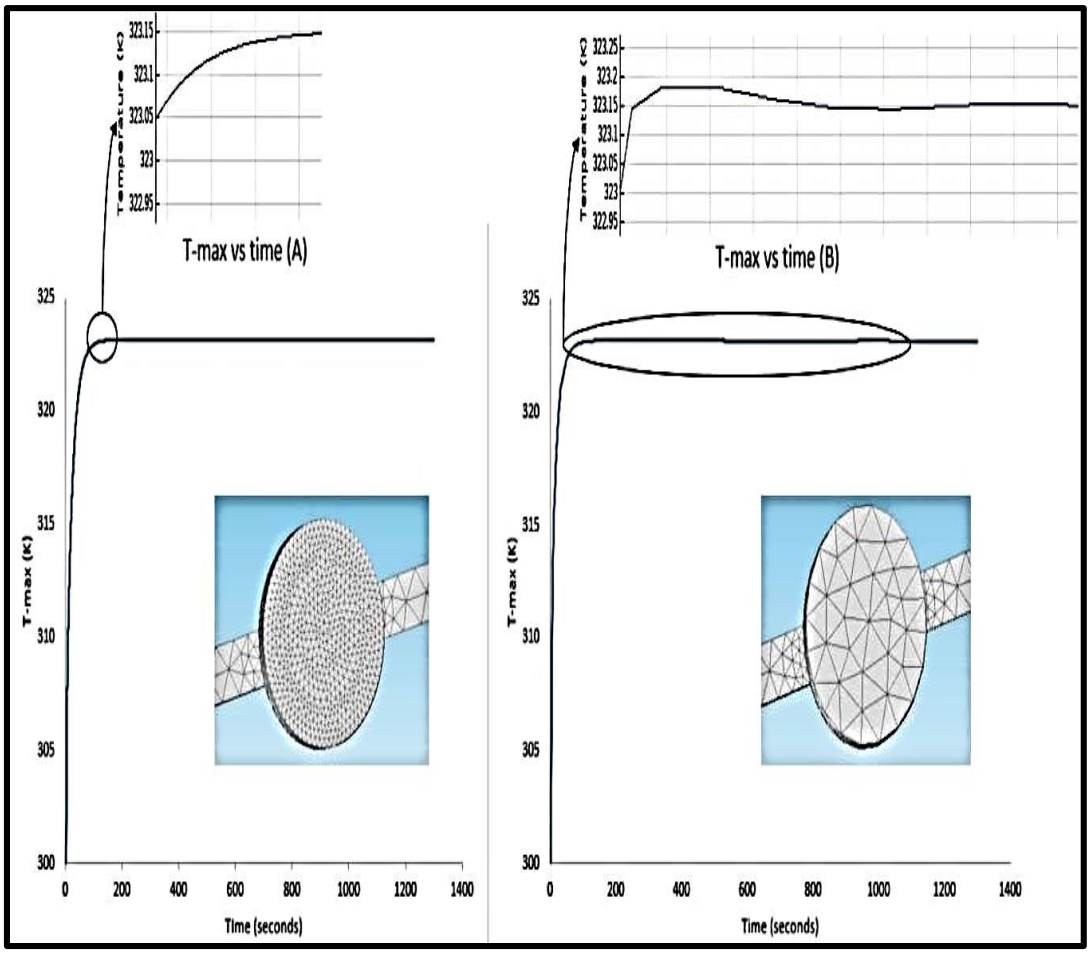

Figure 3.5 T-max vs. time plot for finer mesh vs. extremely coarse mesh at the sensor's surface. The plot on the left shows that by using a finer mesh the t-max at the sensor surface reaches 323.15 and is steady without oscillations. On the right, the unsteady nature of the plot is shown when an extremely coarse mesh is used.

After meshing, the time-dependent study node is selected and the start, stop and time steps in seconds were given, and the computation was initiated. As discussed earlier, initial results showed random oscillations in the data in results and were inaccurate. Hence, the time step was reduced to 0.1s from 1s, solver was made strict from it being a free solver, and the relative tolerance was activated and set to 0.01. These settings gave minimal/no oscillations in the data obtained in results. Parametric sweeps are done along with batch runs for various inlet velocities, a range of depths and positions of the cavity along the microchannel. Results are extracted after the simulation which is the velocity field, average and maximum temperature sensing times of the sensor area.

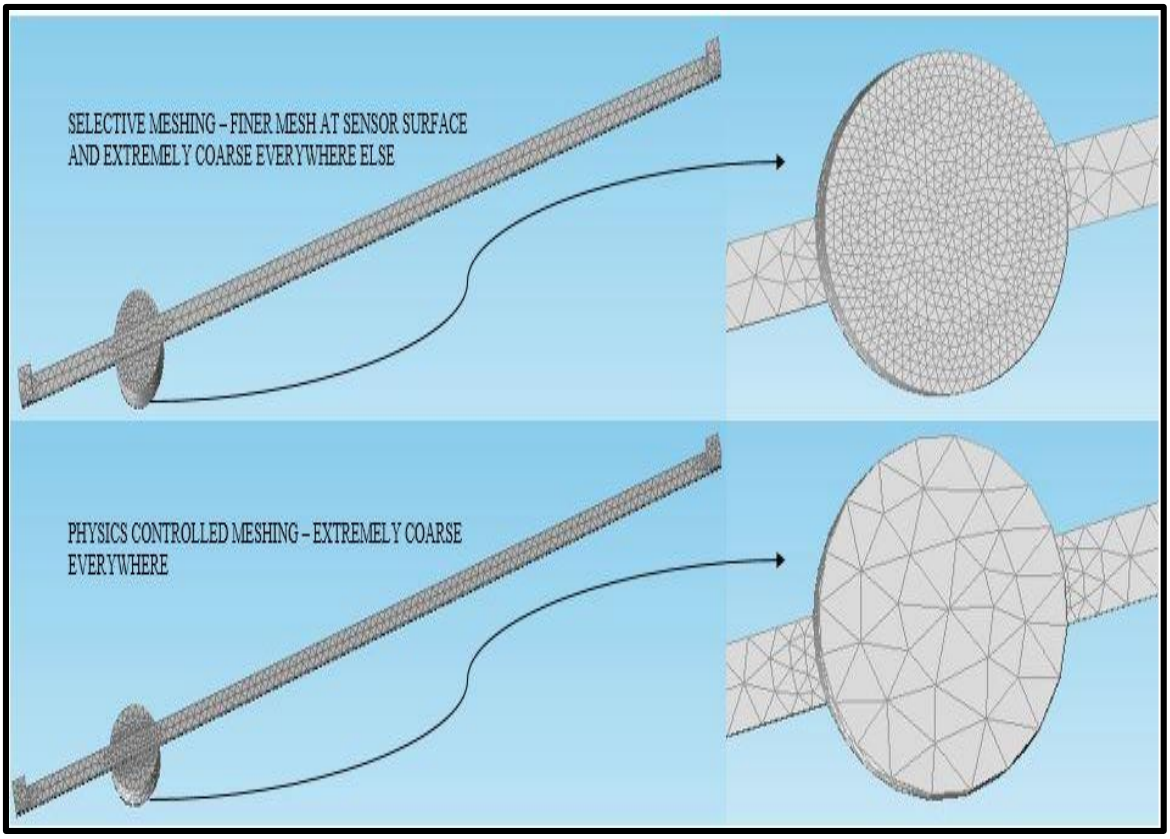

Figure 3.6 Meshing comparison between selective and physics controlled mesh. Comparison of finer mesh and the extremely coarse mesh is shown. Fewer nodes are present in the extremely coarse mesh sensor surface which affects accuracy highly. The finer mesh provides excellent accuracy but comes with heavy computational loads.

3.3 Results and Discussion

The microfluidic device model was set up in COMSOL Multiphysics 5.1 and simulated in it using a computer with the following configuration: i7 processor-2.4GHz, 8 GB RAM,64 bit Windows 10 with 4GB Nvidia GeForce 920M Graphics card.

The parameters used in setting up the model and deriving results from COMSOL Multiphysics are given in the following table.

Table 3.2 Table of Parameters

Dimensions of the microchannel	**Inlet/Outlet radius and height:** 500µm **Channel diameter:** 500µm **Channel depth:** 100µm **Channel length:** 30000µm	
Height of the cavity (H)	**The following heights(µm) were used:** 100,200,300,400,500,600,700,800,900,1000	
Position of the cavity from the inlet (L)	**The following positions(µm) were used:** 5000,10000,15000,20000,25000	
Velocity(m/s)	**Flow rate (ml/hr)**	**Residence time (s)**
10^{-3}	10.8	30
$5*10^{-4}$	5.4	60
10^{-4}	1.08	300
$5*10^{-5}$	0.54	600

The simulation of the microchannel model in COMSOL Multiphysics 5.1 is done to obtain the velocity and temperature profiles. The velocity profile gives an idea of the flow behavior inside the cavity while the temperature profiles provide an idea of the temperature distribution inside the channel and in particular the cavity, which is the focus of this study. The temperature profiles would tell us when the inlet temperature reaches the sensor which is required to understand the sensitivity of the sensor.

The main objective of the simulation is to obtain the best design of the microchannel in which the times to reach the maximum temperature and the average

temperature on the sensor surface is well within the residence times calculated for the particular inlet flow rates.

The time taken for the maximum temperature (t-max) and average temperature (t-avg) to reach the sensor surface is the subject of interest in the simulation. By finding these times, the working range of the sensor is established.

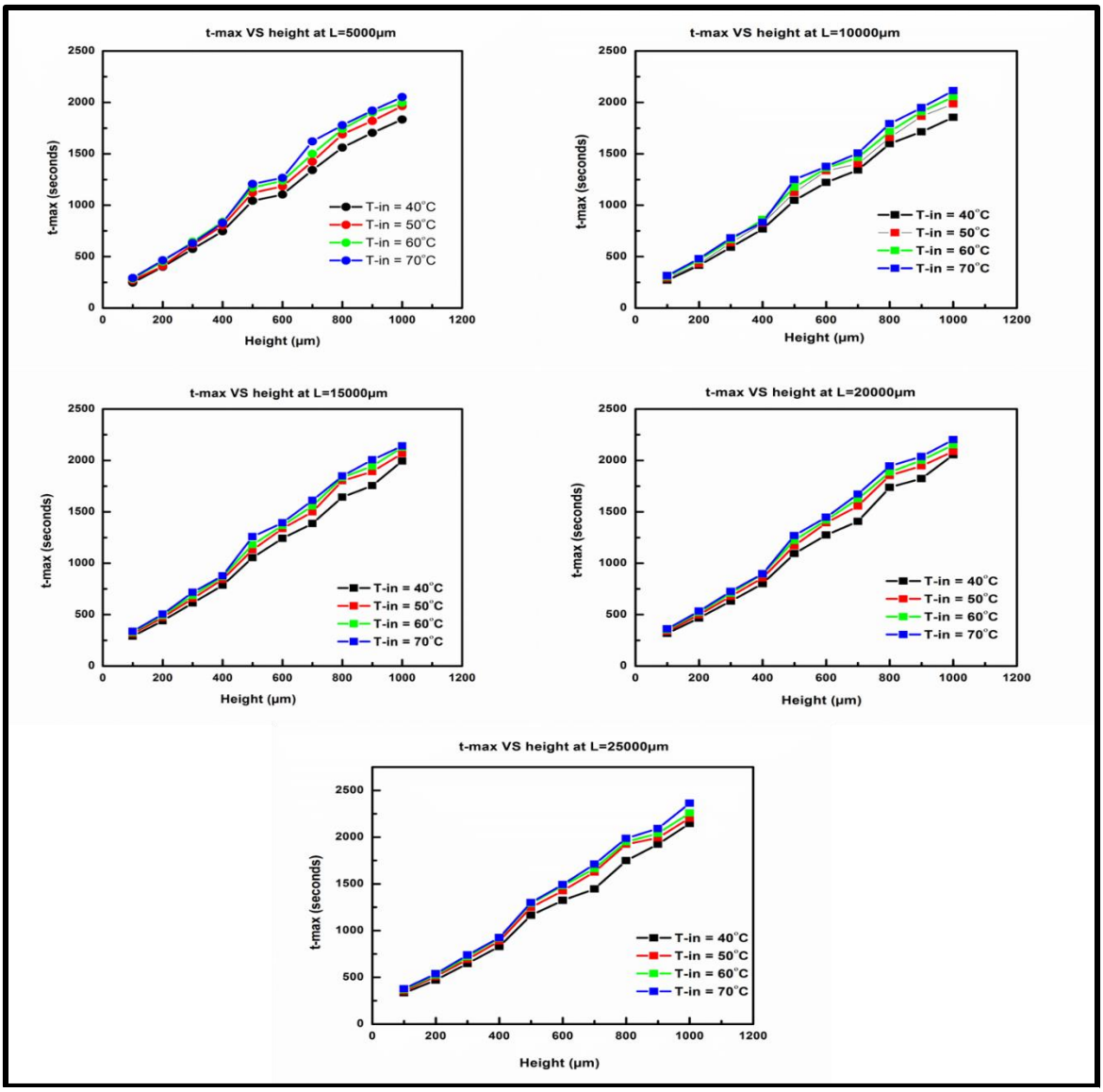

Figure 3.7 Plots for t-max vs height for inlet velocity V = 10^-4 m/s with cavity heights from 100 to 1000 µm and cavity positions: 5000, 10000, 15000, 20000, 25000 µm. The inlet temperature is varied for each run. The plots show a similar trend but with an increasing time.

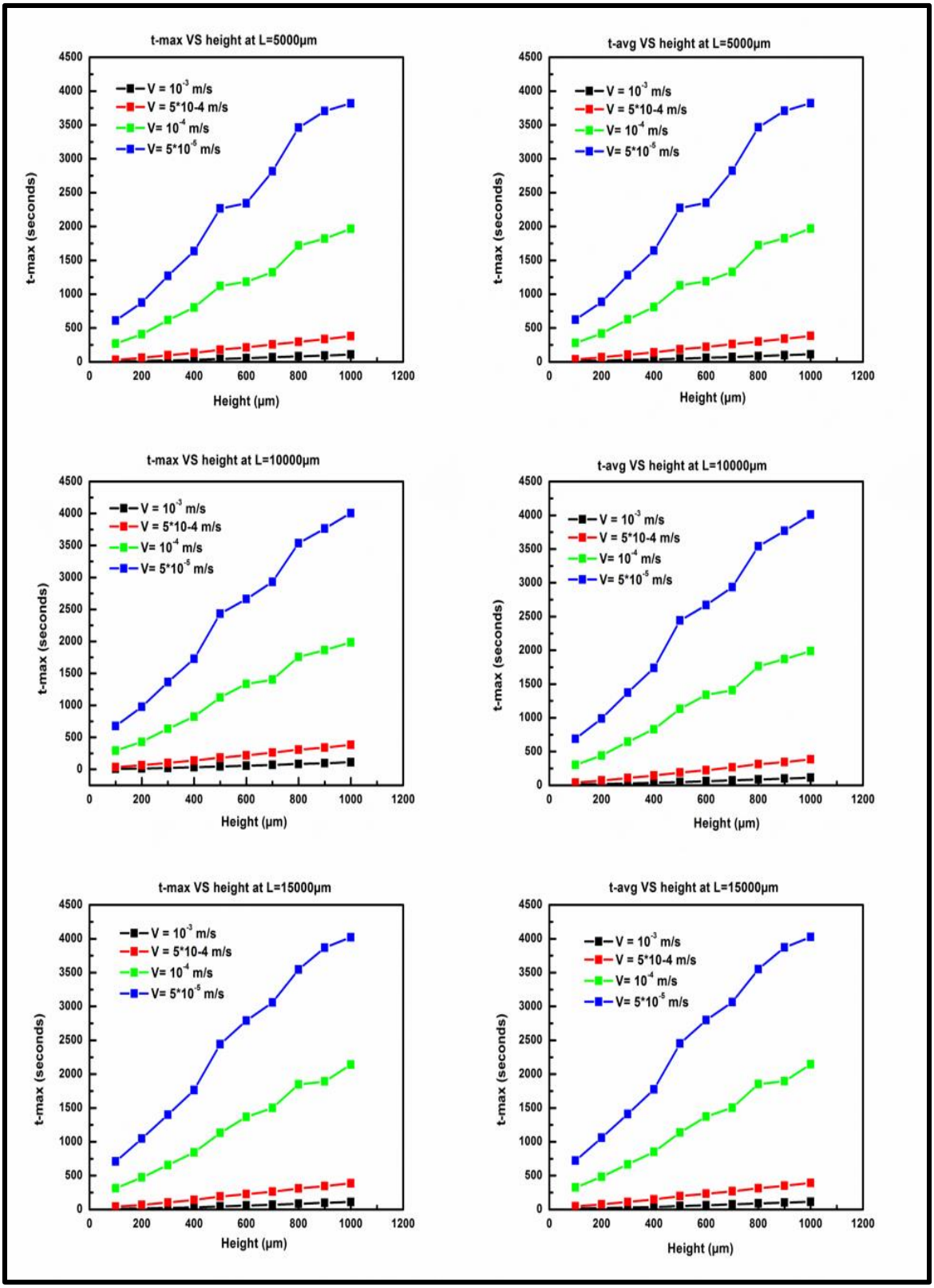

Figure 3.8 Plots for t-max, t-avg vs. heights at various inlet velocities, cavity heights: 100-1000µm and positions: 5000, 10000, 15000. The inlet temperature was set to 323.15 K.

Figure 3.7, shows the plots for t-max vs. heights of the cavity for various inlet temperatures and positions of the cavity at velocity V = 10^{-4} m/s. The plots show no change in the trend with the variation in inlet temperature except that there is a difference in the time to achieve the inlet temperature at the sensor surface.

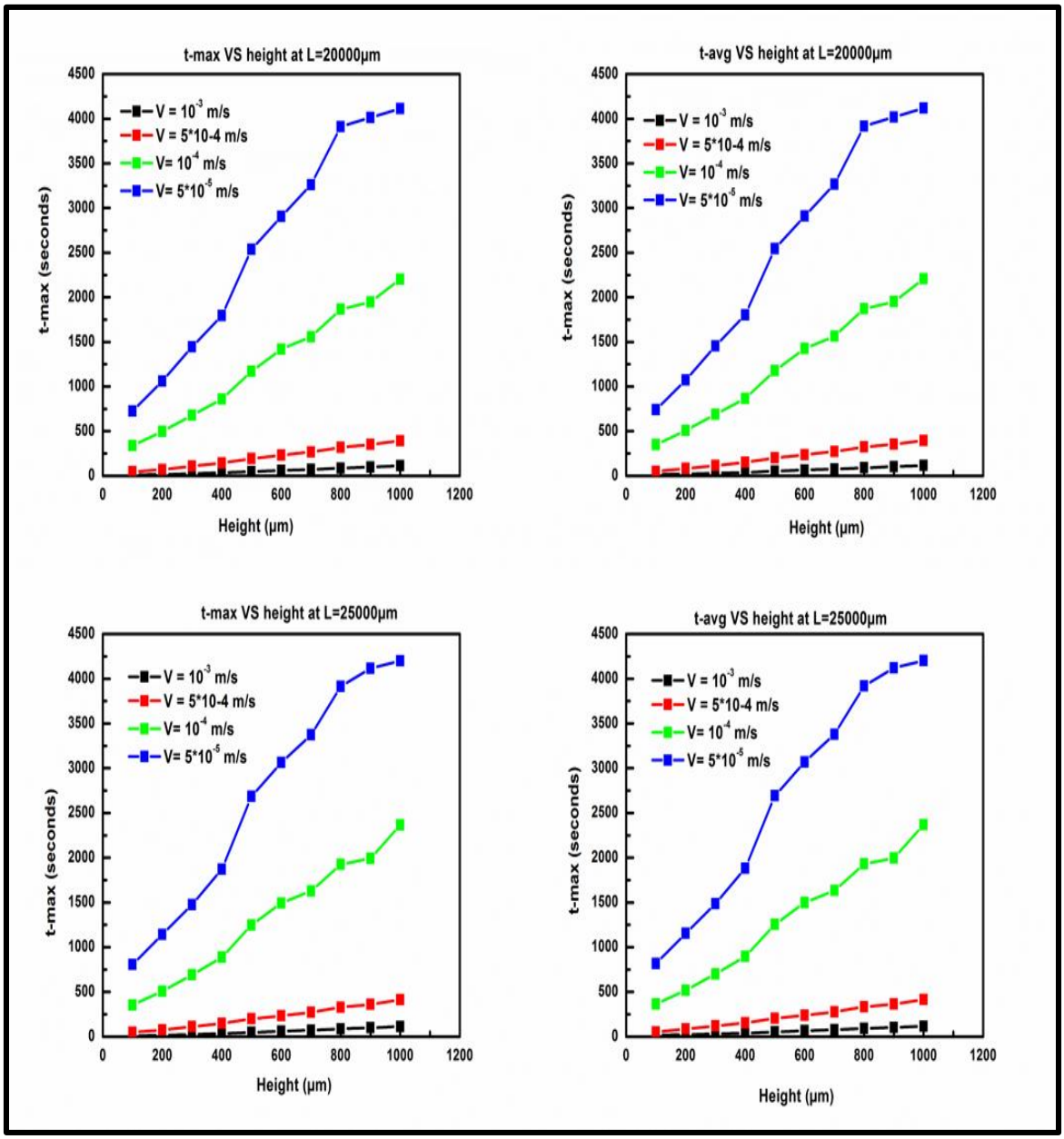

Figure 3.9 Plots for t-max, t-avg vs. heights at various inlet velocities, cavity heights: 100-1000µm and positions: 20000, 25000. The inlet temperature was set to 323.15 K.

Figures 3.8 and 3.9 represent the t-max, t-avg versus the cavity height plots at various cavity positions and velocities. For the velocities V = 10^{-3} and $5*10^{-4}$ m/s, the curve is linear, whereas for lower velocities the linearity vanishes and major variation occurs between heights H = 400-800 µm

Due to the similarity in the trend of t-max vs height plot at various cavity positions and velocities, for detailing a sample plot from Figure 3.8 is shown in Figure 3.10. This is

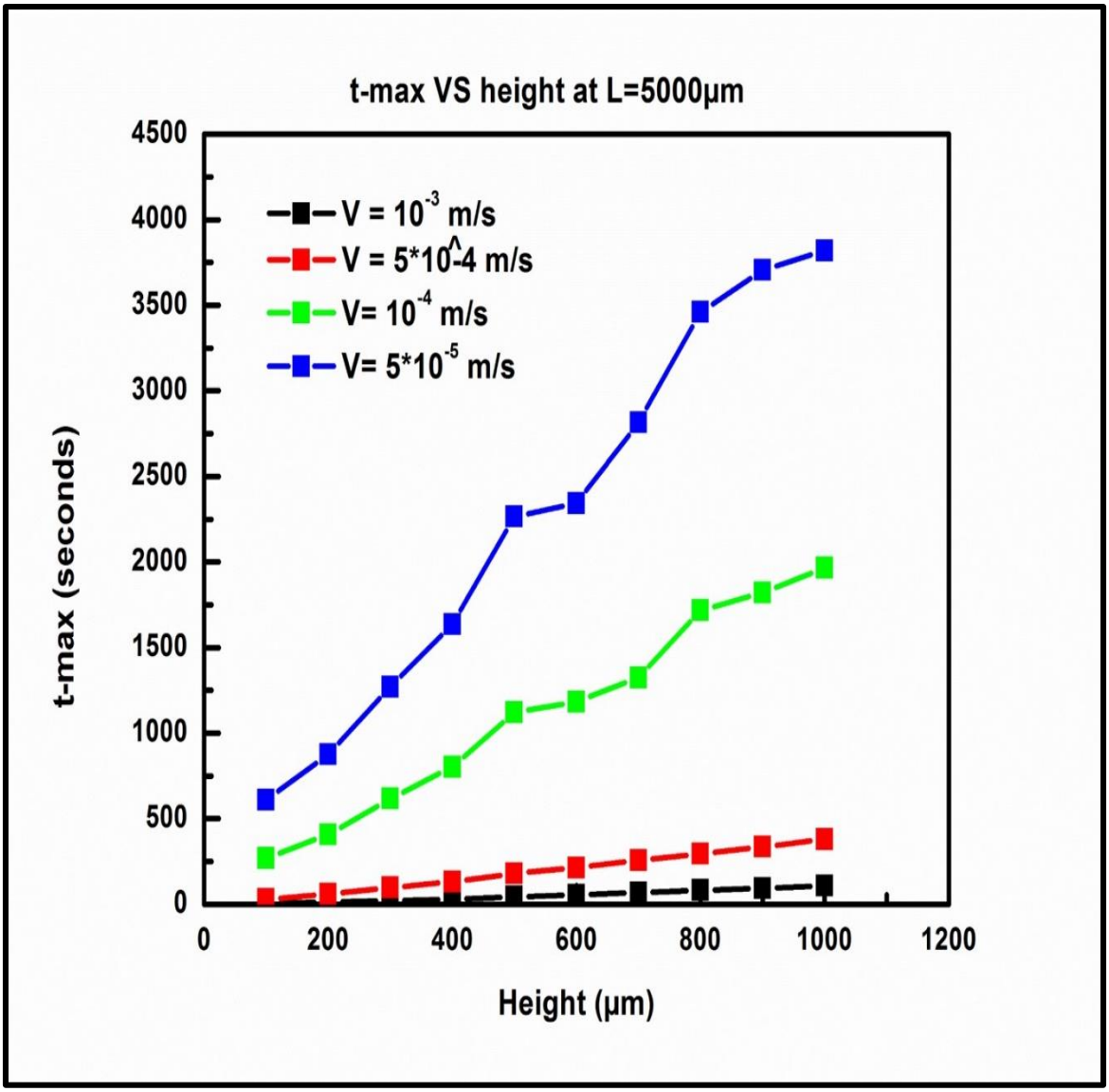

Figure 3.10 Plot for t-max vs. cavity height at cavity position L = 5000µm for various velocities.

a plot of t-max vs cavity heights for the cavity position L = 5000 µm at various velocities. For velocities, V = 10^{-4} and $5*10^{-5}$ m/s, the curve is linear initially from height H = 100 to 400 µm. After H = 400 µm more time is taken to reach the inlet temperature at the sensor surface. The curve then flattens a bit and again increases steeply up to H = 800 µm and flattens out again.

The same trend is observed for plots at the other cavity positions L = 10000, 15000, 20000 and 25000 µm (refer Figures 3.8 and 3.9). The only difference in these plots from the previous plot is that the flat regions becomes steeper as the cavity positions increase.

From the Figures, 3.8 and 3.9, the allowable cavity heights at appropriate lengths for the used velocities was found. For velocity, V=10^{-3}m/s, H=100,200,300 at L=5000, 10000,15000,20000,25000 is allowable. For velocity, V=$5*10^{-4}$m/s, H=100 at L=5000, 10000,15000,20000,25000 is allowable. For velocity, V=10^{-4}m/s, H=100 at L=5000, 10000 is allowable. Suitable H and L at V=$5*10^{-5}$ could not be found. These parameters can be used to fabricate an optimized device.

Figure 3.11, shows the slice side views of the flow profiles and average temperature profiles in the sensor cavity at various times. Similarly, Figure 3.12 shows the average temperature profiles of the sensor surface from the bottom. The heights and cavity positions used to obtain these profiles were, H = 100, 500 and 100; cavity positions L = 5000, 15000 and 25000. A velocity of V = 10^{-4} m/s was used to carry out these runs.

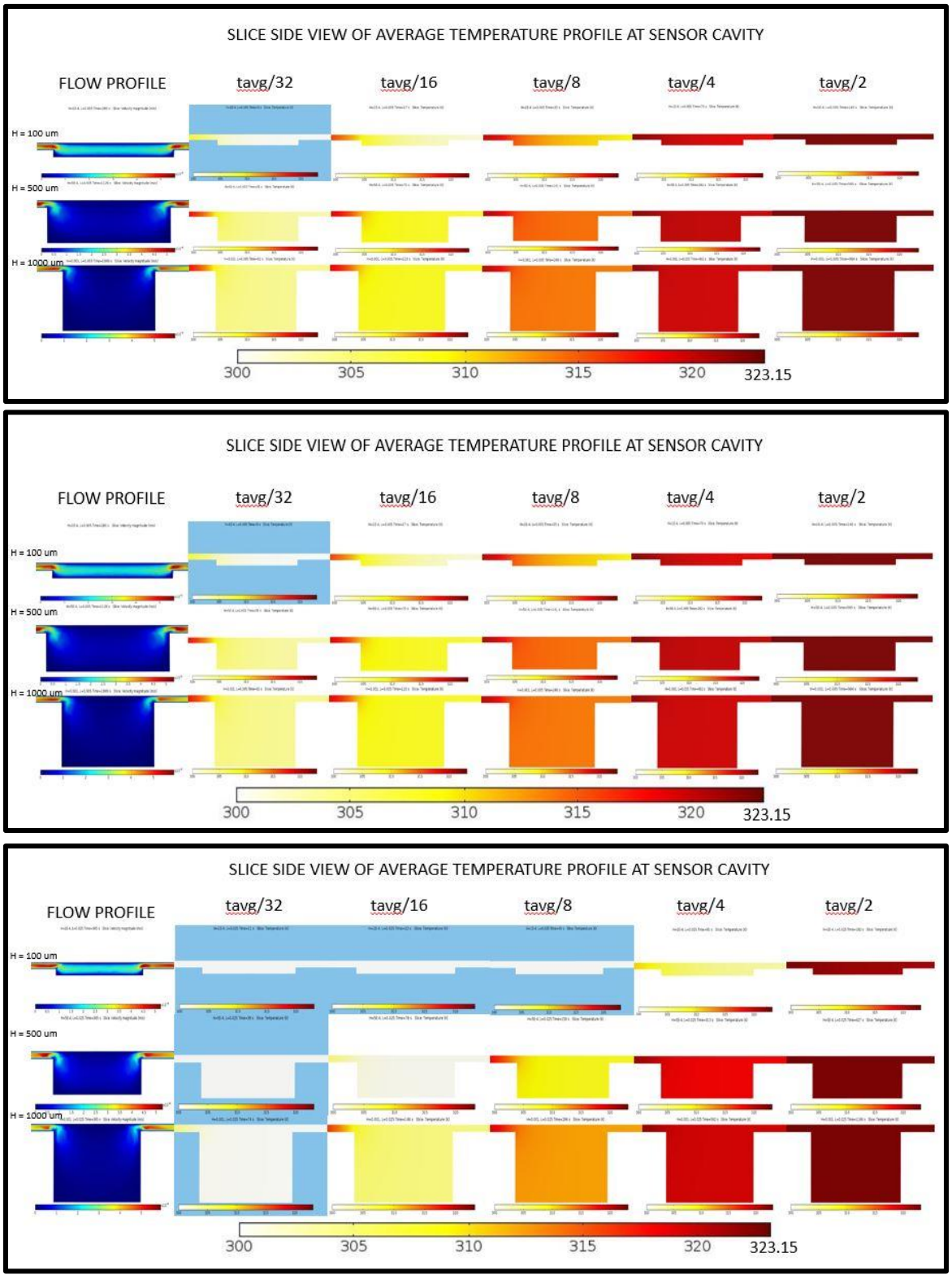

Figure 3.11 Slice side view of the average temperature profile at the sensor cavity for various times. The velocity profile and the average temperature profile is shown for cavity heights: 100, 500, 1000 µm and cavity positions: 5000, 15000, 25000 µm.

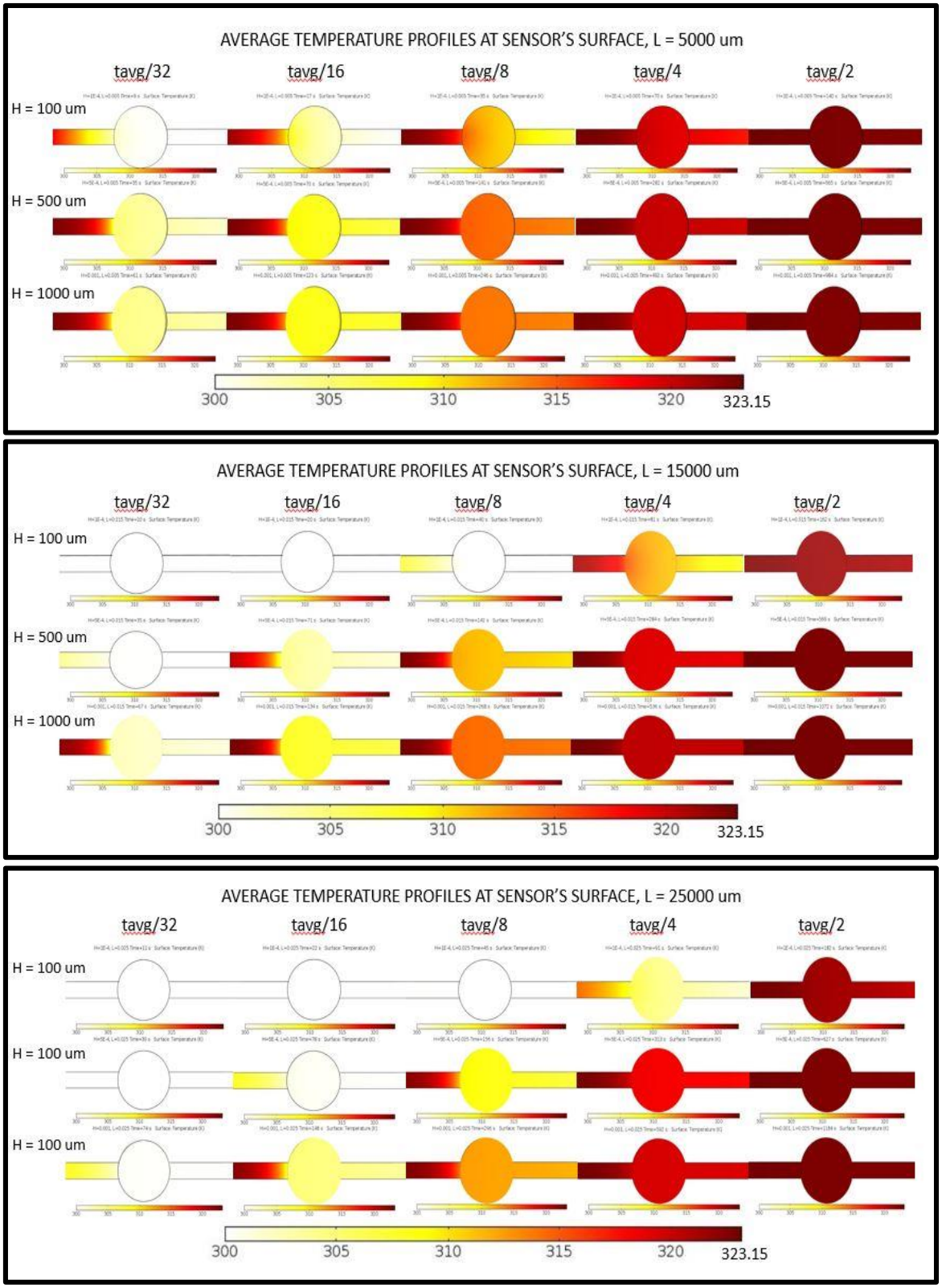

Figure 3.12 Bottom view of the average temperature profile at the sensor surface for various times. The average temperature profile is shown for cavity heights: 100, 500, 1000 μm and cavity positions: 5000, 15000, 25000 μm.

3.4 Sensor Calibration and Validation of Results

A simple calibration model set up is shown in Figure 3.13. Heated or cooled fluid streams of known temperatures are sent into the sensor and a calibration curve is created using the output voltage and the known temperature difference. After the Calibration curve is created, unknown temperature differences can be obtained by relating the obtained output voltage to the corresponding temperature difference in the calibration curve.

After calibration of the temperature sensor, the validation of COMSOL results is done using the following methodology. The sensor device is given fluid streams of known temperatures with inlet velocity of 10^{-4}m/s using syringe pumps. The time taken to reach a steady, required output voltage reading for the corresponding known temperature difference is noted. This value is then compared with the result obtained from COMSOL.

Unfortunately, data from the sensor device could not be obtained by this time and work is currently underway to calibrate the sensor and validate its results with COMSOL.

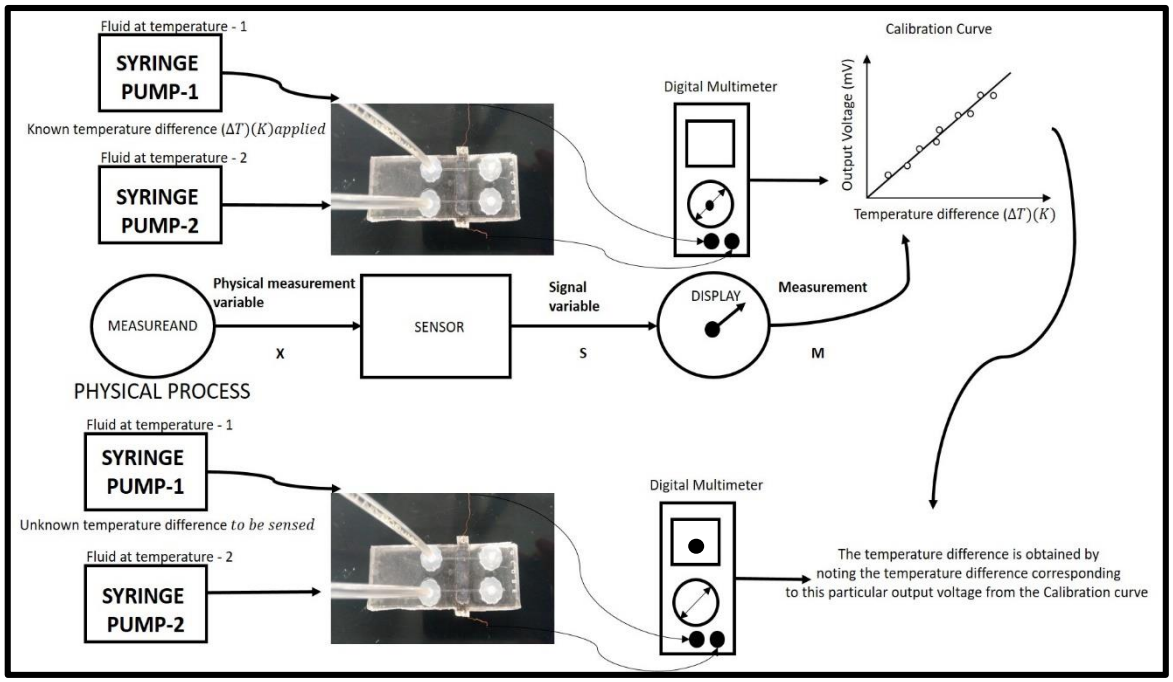

Figure 3.13 A simple temperature sensor calibration model. A calibration curve is created using known temperature differences and its corresponding output voltage. Then, using the calibration curve the unknown temperature difference is obtained.

CHAPTER 4

CONCLUSION

The thesis started with a review of the methods used in temperature sensing and measurements for lab on chip systems in the last 16 years. Even though these methods were useful and efficient, they were costly and involved the usage of heavy equipment or were unable to utilize the method for a lab on a chip system. Due to the need for a cheap, hassle free fabrication of a temperature sensor for lab-on-a-chip systems, the present study dealt with an equipment free, cheap fabrication of a paper based temperature sensor integrated into a microfluidic device, proving it to be suitable for lab-on-a -chip systems.

In the present study, the fluid flow and heat transfer in the device is simulated using COMSOL Multiphysics 5.1. A detailed description of the model set-up and the governing equations with the boundary conditions involved in the model was also put forth, and a successful simulation was brought about.

From the simulation results, the proper dimensions of the microchannel for sufficient temperature sensing in a lab on a chip device was obtained. The temperature distribution and single-phase laminar fluid flow in a microfluidic cavity are also understood from the simulation results. This understanding can also be extended to other thermal microfluidic devices during fabrication.

CHAPTER 5

FUTURE WORK

The motive in the future work is to develop an on-chip sensor to detect explosives using the above-described paper sensor. The design involves two cavities along the length of the microchannel with two sensors, a chemical sensor at cavity one and a temperature sensor at cavity two. The paper based temperature sensor can be transformed into a chemical sensor by depositing or growing chemical sensing materials (Blue, Vobecka, Skabara, & Uttamchandani, 2013) on their surfaces. These materials will produce heat in the presence of target chemicals by bonding with the explosive material atoms/reacting with them which gives out a heat of reaction. This basically would make the chemical sensor a heating element which would heat up the incoming fluid containing the volatile explosive atoms. Then the temperature sensor at cavity two would sense this difference in temperature and give out a potential difference read out. Even though the chemical sensor could itself give out a reading when it detects the explosive material atom, the sensor at cavity two confirms the presence because of the heat produced which is specific to the explosive material interacting with the chemical sensor. Cross-sensitivity with other volatile organic compounds might affect the ability of the chemical sensor in detecting explosive material atoms specifically, thereby making the temperature sensor at cavity two a confirmation on detection. Hence, this sensor chip would prove to be a continuous flow real time accurate explosive detector.

APPENDIX

COMSOL IMPLEMENTATION

To build the model in COMSOL Multiphysics using the governing equations, two physics interfaces are used: the Laminar Flow interface for laminar single-phase fluid flow and the Heat Transfer in Fluids interface for heat transfer. In this model, the equations are coupled in both directions. The Multiphysics nodes Temperature Coupling and Flow Coupling is selected to automatically use velocity and pressure from Laminar Flow into Heat Transfer in Fluids.

MODELING INSTRUCTIONS

Open COMSOL Multiphysics and click **Model Wizard**.

MODEL WIZARD

1. In the **Model Wizard** window, click **3D**.

2. In the **Select physics** tree, select **Fluid flow>Single-Phase Flow>Laminar Flow (spf).**

3. Click **Add**.

4. Click Study.

5. In the **Select study** tree, select **Preset Studies for Selected Physics Interfaces>Time Dependent**.

6. Click **Done**.

DEFINITIONS

Parameters
1. On the **Model** toolbar, click **Parameters**.

2. In the **Settings** window for Parameters, locate the **Parameters** section.

3. In the table, enter the following settings: H = 100um and L =500um (these parameters are useful to do parametric sweeps).

GEOMETRY 1

1. Click geometry and in the settings window set the length unit to µm.

Block 1 (blk 1)
1. On the **Geometry** toolbar, right click and choose **Block**.

2. In the **Settings** window for **Block**, locate the **Size** section.

3. Enter the value 500 for the **height**, **width** and **depth**.

4. In the same **Settings** window, locate **Position** section and enter the following values: X=0, Y=0, Z=100

5. Click the **Build All Objects** button.

Block 2 (blk 2)
1. On the **Geometry** toolbar, right click and choose **Block**.

2. In the **Settings** window for Block, locate the **Size** section.

3. Enter the value 500 for the **height**, **width** and **depth**.

4. In the same **Settings** window, locate **Position** section and enter the following values: X=29500, Y=0, Z=100

5. Click the **Build All Objects** button.

Block 3 (blk 3)
1. On the **Geometry** toolbar, right click and choose **Block**.

2. In the **Settings** window for Block, locate the **Size** section.

3. Enter the values 100, 30000 and 500 for the **height**, **width** and **depth** respectively.

4. In the same **Settings** window, locate **Position** section and enter the following values: X=0, Y=0, Z=0

5. Click the **Build All Objects** button.

Cylinder 1 (cyl 1)
1. On the **Geometry** toolbar, right click and choose **Cylinder**.

2. In the **Settings** window for Cylinder, locate the **Size** section.

3. Enter the values 1000 and H for the **radius** and **height** respectively.

ADD MATERIAL

1. On the **Model** toolbar, right click on **Materials** and select **Add Material** to open the **Add Material** window.

2. Go to the **Add Material** window.

3. In the tree, select **Built-In>Water, liquid.**

4. Click **Add to Component** in the window toolbar and close the **Add Material** window.

MULTIPHYSICS

1. On the **Physics** toolbar, click **Multiphysics** and choose **Global>Temperature Coupling.**

2. On the **Physics** toolbar, click **Multiphysics** and choose **Global>Flow Coupling**.

LAMINAR FLOW (spf)

No changes are done in the default tabs **Fluid Properties 1**, **Initial values 1** and **Wall 1**. The default specifications in these tabs are true to the model in this study. Right click on the **Laminar Flow** tab and select **Inlet** and **Outlet.**

Inlet 1
1. On the **Physics** toolbar, right click and choose Inlet

2. Select Boundary 7 only.

3. In the **Settings** window for **Inlet**, locate the **Velocity** section.

4. The normal inflow velocity is chosen and U_0 is given the values of 10^-3, 5*10^-4, 10^-4, 5*10^-5 m/s (used in this study)

Outlet 1
1. On the **Physics** toolbar, right click and choose **Outlet**.

2. Select Boundary 24 only.

3. In the **Settings** window for **Outlet**, locate the Pressure Conditions section. The default pressure is 0 Pa and remains as such.

HEAT TRANSFER IN FLUIDS (HT)

1. No changes are made in the default tabs**, Heat Transfer in Fluids 1** and **Thermal Insulation 1**.

Initial Values 1
1. In the **Model Builder** window, under **Component 1 (comp1)>Heat Transfer in Fluids (ht)** click **Initial Values 1**

2. In the **Settings** window for Initial Values, locate the Initial Values section.

3. In the T text field, type 300K.

Temperature 1
1. On the **Physics** toolbar, right click and choose **Temperature**.

2. Select Boundary 7 only.

3. In the **Settings** window for **Temperature**, locate the **Temperature** section.

4. In the T_0 text field, type 323.15 (313.15, 333.15, 343.15 K are the other values used in this study)

Outflow 1
1. On the **Physics** toolbar, right click and choose **Outflow**.

2. Select Boundary 24 only.

Heat Flux 1
1. This is used for the special case of studying the temperature profile with PDMS on all boundaries and for the flux just at the sensor surface (resistance concept).

2. On the **Physics** toolbar, right click and choose **Heat Flux**.

3. In the **Settings** window, under the **Equation** section, select the **Convective Heat Flux** option.

4. The **Heat transfer coefficient** is given as 14.79 when the flux is just applied to Boundary 14. (Flux at the sensor surface alone-study)

5. The **Heat transfer coefficient** is given as 15 when the flux is applied to all boundaries except boundary 7 and 24 (PDMS material on all boundaries-study)

6. The **External Temperature** in both cases is set to 300 K.

MESH 1

1. In the **Model Builder** window, under **Component 1 (comp1)** click **Mesh 1** and select **User Controlled Mesh**

Size
1. In the **Settings** window, select **Extremely Coarse Mesh**.

Size 1
1. In the **Settings** window, select **Finer Mesh** and select Boundary 14 only.

2. Click **Mesh 1** and click **Build All**.

STUDY 1

1. Right click on the **Study 1** tab and select **Show Default Solver**.

2. In the Settings window of **Solver Configurations>Solution 1>Time Dependent Solver 1**, under **Time Stepping** change the method of **Steps Taken by Solver** from **Free** to **Strict**.

Step 1: Time Dependent
1. In the **Settings** window of **Study 1>Step 1: Time Dependent**, under **Study Settings** set the **Relative Tolerance** to 0.01

2. The **Times** range is also specified in the format of (Start-time, time step, End-time)

3. Then, the **Compute** button is hit to start the Simulation.

Parametric Sweep
1. Right click on the **Study1** node and select **Parametric Sweep**.

2. In the **Settings** window, add the parameters to be swept (H and L).

3. The **Unit** 'um' is specified and the **Values** needed to be studied are entered in the parameter window.

4. The **Sweep type** is set to **All Combinations** or **Specified Combinations** with respect to the values entered in the Parameter list

5. In the **Study Extensions** option in the **Settings** window, turn '**Off**' the use of **Parametric Solver**.

6. Hit **Compute** in the **Settings** window to start the Simulation.

RESULTS

1. After the Simulation is run, the default plots are generated namely; **Temperature**, **Velocity** and **Pressure**. These nodes are present in the **Results** node.

Surface Maximum and Surface Average
1. Right click on the **Derived Values** node and select **Surface Maximum** and **Surface Average** from the options **Maximum** and **Average** respectively.

2. In the **Settings** window, under **Data**, select the appropriate **Data Set**. Select **Study1/Solution1** if a batch run is done or select **Parametric Solutions1** if a **Parametric Sweep** is done

3. Select Boundary 14 only

4. In the **Expression** tab in the **Settings** window, take '**T**' as the **Expression** and '**K**' as the Unit.

5. Hit **Evaluate** in the **Settings** window, to evaluate the **Surface Average** or the **Surface maximum** at Boundary 14.

6. The **Results** are shown in a table under the **Graphics** window which can be exported as a text file or read then and there.

REFERENCES

Baek, C., Kim, H. Y., Na, D., & Min, J. (2015). A microfluidic system for the separation and detection of E. coli O157:H7 in soil sample using ternary interactions between humic acid, bacteria, and a hydrophilic surface. *Sensors and Actuators B: Chemical, 208*, 238-244. doi: http://dx.doi.org/10.1016/j.snb.2014.11.028

Blue, R., Vobecka, Z., Skabara, P. J., & Uttamchandani, D. (2013). The development of sensors for volatile nitro-containing compounds as models for explosives detection. *Sensors and Actuators B: Chemical, 176*, 534-542. doi: http://dx.doi.org/10.1016/j.snb.2012.10.088

Chon, C. H., & Li, D. (2008). Temperature Control in Microfluidic Systems. In D. Li (Ed.), *Encyclopedia of Microfluidics and Nanofluidics* (pp. 1976-1980). Boston, MA: Springer US.

Darhuber, A. A., Davis, J. M., Troian, S. M., & Reisner, W. W. (2003). Thermocapillary actuation of liquid flow on chemically patterned surfaces. *Physics of Fluids, 15*(5), 1295-1304. doi: 10.1063/1.1562628

De Mello, A. J., Habgood, M., Lancaster, N. L., Welton, T., & Wootton, R. C. R. (2004). Precise temperature control in microfluidic devices using Joule heating of ionic liquids. *Lab on a Chip - Miniaturisation for Chemistry and Biology*, *4*(5), 417-419. doi: 10.1039/b405760k

Erickson, D., Sinton D Fau - Li, D., & Li, D. Joule heating and heat transfer in poly(dimethylsiloxane) microfluidic systems. (1473-0197 (Print)).

Erickson, D., Sinton, D., & Li, D. (2003). Joule heating and heat transfer in poly(dimethylsiloxane) microfluidic systems. *Lab on a Chip - Miniaturisation for Chemistry and Biology, 3*(3), 141-149. doi: 10.1039/b306158b

Guijt, R. M., Dodge, A., van Dedem, G. W. K., de Rooij, N. F., & Verpoorte, E. (2003). Chemical and physical processes for integrated temperature control in microfluidic devices. *Lab on a Chip, 3*(1), 1-4. doi: 10.1039/B210629A

Houssin, T., Cramer, J., Grojsman, R., Bellahsene, L., Colas, G., Moulet, H., . . . Chen, Y. (2016). Ultrafast, sensitive and large-volume on-chip real-time PCR for the molecular diagnosis of bacterial and viral infections. *Lab on a Chip, 16*(8), 1401-1411. doi: 10.1039/C5LC01459J

Hung, M.-S., Ho, C.-C., & Chen, C.-P. (2016). Laser-induced heating integrated with a microfluidic platform for real-time DNA replication and detection. *Journal of Biomedical Optics, 21*(8), 087003-087003. doi: 10.1117/1.JBO.21.8.087003

Jung, W., Han, J., Choi, J.-W., & Ahn, C. H. (2015). Point-of-care testing (POCT) diagnostic systems using microfluidic lab-on-a-chip technologies. *Microelectronic Engineering, 132,* 46-57. doi: http://dx.doi.org/10.1016/j.mee.2014.09.024

Kang, L., Chung, B. G., Langer, R., & Khademhosseini, A. (2008). Microfluidics for Drug Discovery and Development: From Target Selection to Product Lifecycle Management. *Drug Discovery Today, 13*(1-2), 1-13. doi: 10.1016/j.drudis.2007.10.003

Khan, W. A., & Yovanovich, M. M. (2008). Analytical Modeling of Fluid Flow and Heat Transfer in Microchannel/Nanochannel Heat Sinks. *Journal of Thermophysics and Heat Transfer, 22*(3), 352-359. doi: 10.2514/1.35621

Kim, S.-J., Wang, F., Burns, M. A., & Kurabayashi, K. (2009). Temperature-programmed natural convection for micromixing and biochemical reaction in a single microfluidic chamber. *Analytical Chemistry, 81*(11), 4510-4516. doi: 10.1021/ac900512x

Lao, A. I. K., Lee, T. M. H., Hsing, I. M., & Ip, N. Y. (2000). Precise temperature control of microfluidic chamber for gas and liquid phase reactions. *Sensors and Actuators A: Physical, 84*(1–2), 11-17. doi: http://dx.doi.org/10.1016/S0924-4247(99)00356-8

Lee, S. H., Lee Cs Fau - Kim, B.-G., Kim Bg Fau - Kim, Y.-K., & Kim, Y. K. An integrated microfluidic chip for the analysis of biochemical reactions by MALDI mass spectrometry. (1387-2176 (Print)).

Liana, D. D., Raguse, B., Gooding, J. J., & Chow, E. (2012). Recent advances in paper-based sensors. *Sensors (Basel), 12*(9), 11505-11526. doi: 10.3390/s120911505

Liu, D., & Garimella, S. V. (2005). Analysis and optimization of the thermal performance of microchannel heat sinks. *International Journal of Numerical Methods for Heat & Fluid Flow, 15*(1), 7-26.

McDonald, J. C., Duffy, D. C., Anderson, J. R., Chiu, D. T., Wu, H., Schueller, O. J., & Whitesides, G. M. (2000). Fabrication of microfluidic systems in poly(dimethylsiloxane). *Electrophoresis, 21*(1), 27-40. doi: 10.1002/(sici)1522-2683(20000101)21:1<27::aid-elps27>3.0.co;2-c

Miralles, V., Huerre, A., Malloggi, F., & Jullien, M. C. (2013). A Review of Heating and Temperature Control in Microfluidic Systems: Techniques and Applications. *Diagnostics (Basel), 3*(1), 33-67. doi: 10.3390/diagnostics3010033

Morgan, A. J. L., Naylon, J., Gooding, S., John, C., Squires, O., Lees, J., Porch, A. (2013). Efficient microwave heating of microfluidic systems. *Sensors and ActuatorsB:Chemical,181*,904909.doi:http://dx.doi.org/10.1016/j.snb.2013.02.099

Negi, V. S. (2013). *NUMERICAL STUDY OF MICROSCALE HEAT SINKS USING DIFFERENT SHAPES & FLUIDS.* Paper presented at the COMSOL Bangalore, India.

Nery, E. W., & Kubota, L. T. (2013). Sensing approaches on paper-based devices: a review. *Anal Bioanal Chem, 405*(24), 7573-7595. doi: 10.1007/s00216-013-6911-4

Nge, P. N., Rogers, C. I., & Woolley, A. T. (2013). Advances in Microfluidic Materials, Functions, Integration and Applications. *Chemical Reviews, 113*(4), 2550-2583. doi: 10.1021/cr300337x

Oblath, E. A., Henley, W. H., Alarie, J. P., & Ramsey, J. M. (2013). A microfluidic chip integrating DNA extraction and real-time PCR for the detection of bacteria in saliva. *Lab on a Chip, 13*(7), 1325-1332. doi: 10.1039/C3LC40961A

Patsis, G. P., Petropoulos, A., & Kaltsas, G. (2012). Modelling and evaluation of a thermal microfluidic sensor fabricated on plastic substrate. *Microsystem Technologies, 18*(3), 359-364. doi: 10.1007/s00542-011-1409-5

Pitchaimani, K., Sapp Bc Fau - Winter, A., Winter A Fau - Gispanski, A., Gispanski A Fau - Nishida, T., Nishida T Fau - Hugh Fan, Z., & Hugh Fan, Z. Manufacturable plastic microfluidic valves using thermal actuation. (1473-0197 (Print)).

Sackmann, E. K., Fulton, A. L., & Beebe, D. J. (2014). The present and future role of microfluidics in biomedical research. *Nature, 507*(7491), 181-189. doi: 10.1038/nature13118

Selva, B., Jullien, M. C., Miralles, V., & Cantat, I. (2010). Thermocapillary actuation by optimized resistor pattern: Bubbles and droplets displacing, switching and trapping. *Lab on a Chip - Miniaturisation for Chemistry and Biology, 10*(14), 1835-1840. doi: 10.1039/c001900c

Selva, B., Mary, P., & Jullien, M.-C. (2010). Integration of a uniform and rapid heating source into microfluidic systems. *Microfluidics and Nanofluidics, 8*(6), 755-765. doi: 10.1007/s10404-009-0505-7

Singleton, J., Zentner, C., Buser, J., Yager, P., LaBarre, P., & Weigl, B. H. (2013). Instrument-free exothermic heating with phase change temperature control for paper microfluidic devices. *Proceedings of SPIE, 8615*, 86150R. doi: 10.1117/12.2005928

Sun, C., Goharpey, A. H., Rai, A., Zhang, T., & Ko, D. K. (2016). Paper Thermoelectrics: Merging Nanotechnology with Naturally Abundant Fibrous Material. *ACS Appl Mater Interfaces, 8*(34), 22182-22189. doi: 10.1021/acsami.6b05843

Tretheway, D. C., & Meinhart, C. D. (2002). Apparent fluid slip at hydrophobic microchannel walls. *Physics of Fluids (1994-present), 14*(3), L9-L12.

Vigolo, D., Rusconi, R., Stone, H. A., & Piazza, R. (2010). Thermophoresis: Microfluidics characterization and separation. *Soft Matter, 6*(15), 3489-3493. doi: 10.1039/c002057e

Wadgaonkar, I., & Arikapudi, S. Modeling of Humidification in Comsol Multiphysics 4.4.

Whitesides, G. M. (2006). The origins and the future of microfluidics. *Nature, 442*(7101), 368-373. doi: 10.1038/nature05058

Wu, J., Cao, W., Wen, W., Chang, D. C., & Sheng, P. (2009). Polydimethylsiloxane microfluidic chip with integrated microheater and thermal sensor. *Biomicrofluidics, 3*(1), 12005. doi: 10.1063/1.3058587

Xue, Z., & Qiu, H. (2005). Integrating micromachined fast response temperature sensor array in a glass microchannel. *Sensors and Actuators A: Physical, 122*(2), 189-195. doi: http://dx.doi.org/10.1016/j.sna.2005.04.019

Yeo, T., Tan, S. J., Lim, C. L., Lau, D. P. X., Chua, Y. W., Krisna, S. S., . . . Lim, C. T. (2016). Microfluidic enrichment for the single cell analysis of circulating tumor cells. *Scientific Reports, 6*, 22076. doi: 10.1038/srep22076 http://www.nature.com/articles/srep22076#supplementary-information